

**CHARACTERIZATION OF THERMO-PHYSICAL PROPERTIES AND  
FORCED CONVECTIVE HEAT TRANSFER OF POLY-ALPHA-OLEFIN (PAO)  
NANOFLUIDS**

A Thesis

by

IAN CARL NELSON

Submitted to the Office of Graduate Studies of  
Texas A&M University  
in partial fulfillment of the requirements for the degree of

MASTER OF SCIENCE

August 2007

Major Subject: Mechanical Engineering

**CHARACTERIZATION OF THERMO-PHYSICAL PROPERTIES AND  
FORCED CONVECTIVE HEAT TRANSFER OF POLY-ALPHA-OLEFIN (PAO)  
NANOFLUIDS**

A Thesis

by

IAN CARL NELSON

Submitted to the Office of Graduate Studies of  
Texas A&M University  
in partial fulfillment of the requirements for the degree of

MASTER OF SCIENCE

Approved by:

Chair of Committee,  
Committee Members,

Head of Department,

Debjyoti Banerjee  
Dennis O'Neal  
Mahboobul Mannan  
Dennis O'Neal

August 2007

Major Subject: Mechanical Engineering

**ABSTRACT**

Characterization of Thermo-Physical Properties and Forced Convective Heat Transfer of Poly-Alpha-Olefin (PAO) Nanofluids. (August 2007)

Ian Carl Nelson, B.S., The University of Texas

Chair of Advisory Committee: Dr. Debjyoti Banerjee

Colloidal solvents, containing dispersed nanometer (~1-100 nm) sized particles, are categorized as nanofluids. With the growing heat loads in engineering systems that exceed the current technological limits, nanofluids are considered as an attractive option for more efficient heat removal for thermal management applications. Recent results reported in the literature show that the thermo-physical properties of coolants are enhanced considerably when seeded with very minute concentrations of nanoparticles. Hence, nanofluids research has provoked interest in thermal management applications.

The convective heat transfer characteristics of nanofluids are reported in this study. Exfoliated graphite nanoparticles were dispersed in poly-alpha-olefin (PAO) at concentrations of 0.3% and 0.6% (by weight). The heat flux into a convective cooling apparatus was monitored and the results for nanofluid and the base fluid are presented.

Thermo-physical properties of the nanofluid were measured and compared with the base fluid. The thermo-physical properties of the fluid are observed to increase with the addition of the nanoparticles. The specific heat of nanofluid was increased by ~50% compared to PAO. The thermal diffusivity was enhanced by ~400% compared to PAO. The viscosity of the nanofluid was enhanced by 10-1000 times compared to PAO. The

viscosity of the nanofluid was observed to increase with temperature while the viscosity of PAO decreases with temperature. The convective heat flux was enhanced by the nanofluids by up to ~8 % for experiments performed at different heat inputs. The experimental results show that the convective heat transfer enhancement potentially results from the precipitation of nanoparticles on the heated surface and results in enhanced heat transfer surfaces (“nano-fins”).

To

My parents and my sister and brother

## ACKNOWLEDGEMENTS

I would like to thank my research advisor and committee chair, Dr. Banerjee, for his continual guidance, support, and interest in my studies and the achievement of this work. I have learned much under his direction and instruction and highly value the time as a graduate student under his advisory. I would also like to thank Dr. M. S. Mannan, and Dr. D. O'Neal for being a part of my thesis committee.

I would like to express my gratitude to Dr. R. Ponnappan at the Air Force Research Labs in Dayton, Ohio for his overall guidance of this project and his help in acclimating me with the many procedural encumbrances associated with research at the Air Force Research Labs for a visiting student. I also acknowledge the support of Dr. Kirk Yerkes of AFRL, Dr. Lanchao Lin, Dick Harris, and Roger Carr of UDRI for their help and gracious accessibility for my many questions. I would like to thank Dr. Lafdi (UDRI) for his preparation of the nanofluids and measurement of the viscosity and thermal diffusivity. Additionally, Dr. Ganguly, and Dr. A. Roy helped with the specific heat measurements. I also acknowledge the Universal Technology Corporation for their supporting my summer position in Dayton.

Finally I would like to thank my family and friends, and all the others who supported me in any number of ways during my studies and work as a graduate student in College Station.

## TABLE OF CONTENTS

	Page
ABSTRACT .....	iii
ACKNOWLEDGEMENTS .....	vi
TABLE OF CONTENTS .....	vii
LIST OF FIGURES .....	ix
LIST OF TABLES .....	xi
NOMENCLATURE .....	xii
 CHAPTER	
I INTRODUCTION .....	1
1.1 Thesis Introduction.....	1
1.2 Nanofluid Historical Development .....	3
1.3 Fluidic Thermal Conductivity.....	3
1.4 Pool Boiling Experiments.....	6
1.5 Forced Convection Experiments.....	8
1.6 Carbon Nanotube (CNT) Suspensions.....	13
1.7 Summary of Nanofluid Experimental Results.....	15
1.8 Project Background .....	17
 II DESCRIPTION OF EXPERIMENTAL APPARATUS .....	 18
2.1 Experimental Apparatus Introduction .....	19
2.2 Flow Loop Apparatus.....	19
2.3 Flow Loop Instrumentation.....	22
 III EXPERIMENTAL PROCEDURE .....	 24
3.1 Test Parameters .....	24
3.2 Data Collection.....	25
3.3 System Flushing Procedure.....	26
3.4 Measurement Uncertainty .....	27

CHAPTER	Page
IV NANOFUID CHARACTERIZATION .....	29
4.1 Nanoparticle and Nanofuid Manufacture.....	29
4.2 SEM Analysis.....	29
4.3 EDX Analysis.....	31
V RESULTS AND DISCUSSION .....	33
5.1 Thermal Property Analysis.....	33
5.2 Baseline Test Results .....	38
5.3 Nanofuid Test Results .....	43
5.4 Nanofuid Test Analysis.....	47
VI CONCLUSION .....	52
REFERENCES.....	54
GLOSSARY .....	59
APPENDIX .....	60
VITA .....	68



## LIST OF FIGURES

FIGURE	Page
1 Schematic of the flow loop apparatus showing the test section (cooling chamber) with the offset fin array. ....	18
2 Diagram of copper fin array showing flow direction and offset fin configuration. ....	19
3 Schematic of fin array, substrate, and steel plate assembly drawing showing thermocouple placement and solder points. ....	20
4 Scanning Electron Microscopy (SEM) image showing precipitated nanoparticles. The exfoliated graphite nanoparticles appear semi-transparent in the image and are indicated by superposed arrows in the image. ....	30
5 Scanning Electron Microscopy (SEM) image showing surface agglomeration of the precipitated exfoliated graphite nanoparticles that were deposited on the fin surface. ....	31
6 EDX (Energy Dispersive X-Ray) spectra of copper (Cu) fin surface performed after the experiments showing elemental surface deposition of carbon (C). ....	32
7 Viscosity measurements for PAO and nanofluid (0.6% concentration by weight). ....	34
8 Specific heat measurements for PAO and nanofluid (0.6% concentration by weight). ....	35
9 Thermal diffusivity measurements for PAO and nanofluid (0.6% concentration by weight). ....	37
10 Thermal conductivity measurements for PAO and nanofluid (0.6% concentration by weight). ....	38
11 Variation of $Nu/Pr^{1/3}$ with Reynolds number for flow through both gap-fin and non-gap offset fin array. Weiting's correlation <sup>49</sup> is plotted for comparison with the experimental data. ....	41

FIGURE	Page
12 Variation of $Nu/Pr^{1/3}$ with Reynolds number using PAO for the experimental apparatus before being exposed to the nanofluid and after exposure to the nanofluid. ....	42
13 Heat flux as a function of flow rate for both nanofluid concentrations and pure PAO for a heat input of 300 W. ....	43
14 Heat flux as a function of flow rate for both nanofluid concentrations and pure PAO for a heat input of 400 W. ....	44
15 Heat flux as a function of flow rate for both nanofluid concentrations and pure PAO for a heat input of 500 W. ....	45
16 Comparison of PAO to 0.6% PAO nanofluid using Weiting correlation at 300W input. ....	48
17 Comparison of PAO to 0.6% PAO nanofluid using Weiting correlation at 400W input. ....	48
18 Comparison of PAO to 0.6% PAO nanofluid using Weiting correlation at 500W input. ....	49
19 Comparison of the ratio of Nu and ratio of the $(RePr^{1/3})$ at a 300 W input.....	50
20 Comparison of the ratio of Nu and ratio of the $(RePr^{1/3})$ at a 400 W input.....	50
21 Comparison of the ratio of Nu and ratio of the $(RePr^{1/3})$ at a 500 W input.....	51

**LIST OF TABLES**

TABLE	Page
1 Summary of nanofluid heat transfer experiments reported in the literature.....	15
2 Relationship between the ratio of Nu and ratio of the $(\text{RePr}^{1/3})$ at 300 W input.....	51
3 Relationship between the ratio of Nu and ratio of the $(\text{RePr}^{1/3})$ at 400 W input.....	51
4 Relationship between the ratio of Nu and ratio of the $(\text{RePr}^{1/3})$ at 500 W input.....	51

**NOMENCLATURE**

$\varphi$	Volume Fraction
$\Omega$	Flow Characteristic
$T_{b,m}$	Mean Temperature of Fin Base
$T_{s,m}$	Mean Temperature of Substrate
$q$	Heat Flux
$t_s$	Substrate Thickness
$k_s$	Solid Thermal Conductivity
$\alpha_l$	Liquid Thermal Diffusivity
$k_l$	Liquid Thermal Conductivity
$\rho_l$	Liquid Density
$c_{p,l}$	Liquid Constant Pressure Specific Heat
$n_f$	Number of Fins per Strip
$n_{st}$	Number of Fin Strips
$h$	Heat Transfer Coefficient
$P$	Fin Perimeter
$A_c$	Fin Cross Sectional Area
$l$	Fin Length in Flow Direction
$D_h$	Hydraulic Diameter
$U$	Velocity
$\mu$	Viscosity

$a$  Height of Rectangular Duct

$b$  Width of Rectangular Duct

## CHAPTER I

### INTRODUCTION

#### 1.1 Thesis Introduction

Thermal management of high heat flux engineering systems has been the contemporary topic of interest in both the industry and the academic research communities. Cooling needs of high heat flux devices have outgrown the thermal management solutions developed in the past few decades. These high heat flux devices are now being limited in performance and range by the lag in heat removal capabilities of existing cooling systems. Many applications, including the cooling of electronics, necessarily produce high enough heat fluxes to stretch the current thermal management methods and are now driving the advances in heat transfer augmentation methods.

Since the discovery of carbon nanotubes in the late 1970's<sup>1</sup> and the realization of their potential some years later<sup>2</sup>, nano-science has been of great interest to various research communities. The promise of early results from nano-science research in almost every field has come with much anticipation of how current technologies will be transformed in the future due to nanotechnology. One such area of nano-science currently of interest to thermal research is the topic of "nanofluids". Colloidal solvents containing dispersed nanometer (~1-100nm) sized particles are categorized as nanofluids. Compositions of solid and liquid particles have been studied since the 1970's, but not until the incorporation of nanometer sized particles have these

---

This thesis follows the style of *American Institute of Aeronautics and Astronautics Journal*.

compositions attracted significant attention from the thermo-fluids research community. Anomalous enhancement in thermo-physical properties have been reported in the literature when the particles used to seed the base fluids were changed from micrometer-sized particles to nanometer-sized particles.

Thermal conductivity enhancements in nanofluids have been reported by up to 150%<sup>3</sup> and critical heat flux (CHF) enhancement of up to 200%<sup>4</sup> have been reported when compared to the corresponding properties and CHF values of base fluids. The enhancements are produced at low nanoparticle concentrations of less than 4% with nanoparticle sizes ranging from 10 - 100 nm. Results from various models have been found to be inadequate in accounting for the results reported in the literature for the anomalous enhancements observed in transport properties of nanofluids.<sup>5</sup>

Superior thermal management technology will be necessary in future Air Force instrumentation as the current characteristics of conventional heat transfer fluids will be inadequate for meeting the future thermal loads of on-board air-craft systems. Nanofluids for thermal management are therefore a rapidly growing area of research. Nanofluids in cooling systems can potentially decrease the weight and size of ground as well as space based thermal management systems without requiring significant process or tooling modification. Settling, abrasion and clogging are not encountered with nanofluids due to the small nanoparticle sizes, allowing their seamless incorporation in current thermal management systems. Nanofluids enable a more efficient, effective and uniform heat removal capability for systems requiring highly accurate temperature control at high heat fluxes.

## 1.2 Nanofluid Historical Development

A nanofluid<sup>6</sup> is defined as a colloidal solvent containing dispersed nanometer (~1-100 nm) sized particles. Enhancements in thermal conductivity were discovered for nanofluids with low nanoparticle concentrations (< 4%). A wide range of enhancements in thermal conductivity were reported for nanofluids based on the material, concentration, size and aspect ratio of the nanoparticles as well as the base fluid, pH of aqueous solutions and the presence and type of stabilizers<sup>7</sup>. The classical theories developed for thermal conductivity of heterogeneous colloidal mixtures predict lower enhancements than observed in experimental data for nanofluids. Predictions by the classical compositional models<sup>3,8</sup> (such as the Hamilton and Crosser<sup>9</sup> model) were found to be inconsistent with the experimentally observed enhancement of the thermal conductivities of the nanofluids.

## 1.3 Fluidic Thermal Conductivity

The term nanofluid was first coined by Choi (1995)<sup>10</sup> where he described the future and hope of this application of nanotechnology. His subsequent work in 2001<sup>3</sup> presented results showing thermal conductivity enhancement of up to 150% for nanofluid compared to pure fluid. In this study<sup>3</sup>, Choi reported the results for nanofluids using multi-walled carbon nanotubes (MWNT) suspended in PAO. The thermal conductivity measurements were performed using the transient hot-wire (THW) method where a thin electrical wire is immersed vertically into the test fluid. Short duration, high-energy pulses are sent through the wire and its time dependent temperature variation is monitored continuously in the experiments. The normalized thermal



conductivity is presented as a function of the suspended particle loading, within the range of 0-1% by volume fraction. Most notably, the nanofluid thermal conductivities were found to vary non-linearly as a function of the nanoparticle loading. Choi<sup>3</sup> proposed that the observed enhancement in thermal conductivities were due to the surface organizations of the liquid molecules on nanoparticles and due to ballistic heat transfer through the particle. He further proposed that the nonlinear variation of thermal conductivity on concentration depends on the number of nanotubes in the solution and the extremely high aspect ratio of these nanotubes.

Other researchers studying the effects of nanofluids also reported significant enhancement in thermal conductivities. Eastman et al.<sup>8</sup> reported the effect of metallic nanoparticles dispersed within ethylene glycol for nanoparticle solutions ranging in concentration of up to 0.5% by volume containing CuO nanoparticles. This group's previous work<sup>11</sup> had shown an increase in thermal conductivities on the order of 20% for a 4% by volume solution of CuO and Al<sub>2</sub>O<sub>3</sub> nanoparticles suspended in ethylene glycol. In these experiments the nanofluids that were stabilized using thioglycolic acid yielded the highest enhancement of 40% for 0.3% by volume concentration of nanoparticles. The authors then compared the experimental data with analytical model for the thermal conductivity of two component mixtures proposed by Hamilton and Crosser<sup>9</sup>. The results showed that the analytical models dramatically under-predicted the values of thermal conductivity of nanofluids compared to experimental data. The disparities between the predictions by analytic models and the experimental results for the thermal conductivities of the metallic nanofluids differ by an order of magnitude (up to ten

times). The authors presented two possible weaknesses in the Hamilton and Crosser model that may account for the observed disparities in predictions. First, the model does not consider the role of particle size on the thermal conductivity and second, it fails to show a strong dependence of particle thermal conductivity on the overall thermal conductivity.

A similar paper<sup>12</sup> reported experimental data on the effects of SiC nanoparticles (26 nm diameter) immersed in an aqueous solution. The thermal conductivity of the fluid was found to increase by 15.8% at a volume fraction of 4.2% and was measured using the THW method. A comparison was similarly made with the predictions by the Hamilton Crosser model. However, large discrepancies were observed between predictions and the experimental data.

Recently reported data and proposed theories suggest that the enhancements in thermal conductivity are potentially due to localized Brownian convection<sup>13</sup>. This is validated by the analysis of various experimental data for aqueous nanofluids which show a range of thermal conductivity enhancement that are observed to depend on the nanoparticle size. The competing effects of two transport resistances govern the range of spherical nanoparticle diameters (10-50 nm). The larger bound is proposed to be the result of Brownian convection<sup>13</sup>, whereas the lower bound is proposed to be the effect of liquid-solid interfacial resistance on the nanoparticle surface<sup>14</sup>. These competing effects could explain the maxima reported in thermal conductivity enhancement of nanofluids. Additionally, the enhancement could be explained by surface coating of precipitated

nanoparticles on the measurement probes. Studies conducted on the thermal conductivity of nanofluids have not addressed the effect of nanoparticle precipitation.

#### **1.4 Pool Boiling Experiments**

Enhancements in two-phase convective heat transfer were reported for nanofluids<sup>5,7</sup>. An experimental study of CHF during pool boiling of nanofluids was conducted by You et al<sup>4</sup>. Concentrations of alumina ( $\text{Al}_2\text{O}_3$ ) ranging from 0 g/L to 0.5 g/L were studied and their pool boiling curves were presented. The curves show the CHF to increase by up to 200% for the saturated nanofluid when compared to pure water. The average size of bubbles increased in the nanofluid and the frequency of the bubbles decreased. The results are compared to the Zuber model<sup>15</sup> and shown to be dramatically underestimated by the prediction. The authors opined that the Zuber prediction considers only the heat of vaporization, density of vapor and liquid, and surface tension in prediction of the CHF.

A similar study<sup>16</sup> also reported results from boiling heat transfer experiments using 80-100 nm diameter copper nanoparticles with acoustic cavitation. The study found that with generation of an acoustic field, the heat transfer was enhanced in Cu nanofluid, and that the enhancement was independent of the heat flux. The acoustic energy and fluid subcooling did not alter the heat transfer of the liquid when copper nanoparticles were not added. The heat transfer enhancement was primarily attributed to the thermophysical properties of the nanoparticles.

While these studies mentioned above demonstrated enhancement in heat transfer with nanoparticle addition in pool boiling, one group reported no such increase. The

paper<sup>17</sup> presents the results of a pool boiling experiment using nanofluids as the heat transfer medium. From the pool boiling experiments, it was reported that the overall heat transfer deteriorated as the particle size of the nanofluid was increased, such that when compared to the base fluid, the heat transfer in the nanofluid was lower. Because of this reduction in heat transfer through the nanofluid in a pool boiling experiment, the authors suggest that nanofluids should not be used as a solution to the growing need for high heat flux thermal management.

Similarly, another group also reported that heat transfer was not increased with nanoparticle addition. Vassallo et al.<sup>18</sup> also reported that while heat transfer was not increased, the CHF of the solution was increased. In this study, pool boiling experiments were conducted using silica-water nanofluids to explore the effect on heat transfer characteristics of the setup including the CHF in pool boiling. The experimental setup consisted of a Pyrex bowl filled with the coolant (i.e. the nanofluid or water). A NiCr wire was then submerged within the fluid and current was passed through the wire. The bulk temperature of the solution was measured using a thermocouple, and the Pyrex bowl was heated with a hot plate apparatus. The experiments were run until CHF was reached or until the test wire broke. The resistance of the wire was measured using the voltage and current variance. From this resistance value, the heat flux through the wire was then obtained. The results demonstrate that there is minimal effect of particle concentration on the heat flux. The experiments were performed using a solution of silica nanoparticles. However, the CHF for the nanofluids were higher than the base fluid.

The enhancements in CHF for the pool boiling experiments with nanofluids is possibly due to an increase in the number of nucleation sites, the size of nucleation cavities, and the associated nucleation site density arising from the precipitation of nanoparticles. Therefore, a systematic study on the effect of surface precipitation of nanoparticles during pool boiling experiments is needed to clarify the conflicting results reported in the literature.

### **1.5 Forced Convection Experiments**

Apart from thermal conductivity measurements, subsequent studies were focused on ascertaining the convective transport properties of nanofluids. Through the conductivity measurements described before, researchers were able to determine the relationships between thermal conductivity and particle suspension stability, particle material and size, concentration, as well as temperature. The next logical step in the research on nanofluids was to test the convective transport efficacy in an internal flow loop. To determine the convective transport characteristics of the nanofluid, the natural and forced convective heat transfer coefficients were measured in these studies.

A study<sup>19</sup> of aqueous solutions using  $\gamma$ -Al<sub>2</sub>O<sub>3</sub> and TiO<sub>2</sub> nanoparticles sized 13 and 27 nm, respectively, reported viscosity values 200 times higher than for water. The experimental setup consisted of a 480 cm long pipe with an inner diameter of 1.07 cm. The nanofluid loading was 10% volume concentration for both the alumina and titanium oxide nanofluids. The Darcy friction factor of the nanofluids was measured to be within 3% of water at an equivalent Reynolds number. This finding is similar to other published data<sup>21</sup> that found the friction factor of 100 nm Copper nanofluids to be the

same as water at an equivalent Reynolds number. The nanofluid was also compared to water based on the same velocity. Because of the significant increase in viscosity of the nanofluid, the pumping loss was 31% higher and the friction factor was calculated to be 36% higher than water. Pak and Cho propose a Nusselt number correlation for turbulent flow in a pipe as,

$$Nu = 0.021Re^{0.8} Pr^{0.5} \quad (1)$$

based on the heat flux data collected from the experiment. The heat flux is found to be 12% lower for the nanofluids than water based on the constant velocity of the flow.

A nanofluid consisting of CuO nanoparticles at a loading of 0.9% by volume concentration in an aqueous solution was reported to enhance the forced convection heat transfer coefficient by 15%<sup>20</sup>. The effect of nanofluid on the forced convective heat transfer was reported by Xuan and Li<sup>21</sup>. In this study a test section with temperature measurements at the inlet and outlet, and periodic temperature measurements at corresponding locations on the inside and outside diameter was performed in order to observe the heat transfer coefficients and heat fluxes using nanofluid coolant. The inlet temperature was kept at a constant temperature using a high capacity chiller. The nanofluid consisted of copper particles of diameter less than 100 nm suspended in deionized water (DW) with a concentration by volume ranging between 0.3% and 2.0%. The Nusselt number was found to increase with increasing Reynolds number (10,000-25,000) and nanoparticle loading and was reported to be 60% higher than water for equivalent Reynolds numbers at a loading of 2% volume concentration. Based on the experimental results, the authors developed a correlation for calculating the Nusselt

number of this nanofluid. A new correlation was presented based on Peclet, Reynolds, and Prandtl numbers of the particles and nanofluid respectively:

$$Nu = c_1 (1.0 + c_2 \phi^{m_1} Pe_d^{m_2}) Re_{nf}^{m_3} Pr_{nf}^{0.40} \quad (2)$$

where the subscript *nf* refers to the effective nanofluidic properties,  $\phi$  is the volume fraction, and  $c_1, c_2, m_1, m_2, m_3$  are the correlation constants. The friction factor of the fluid was also studied by measuring the pressure drop through the system with a digital manometer. The results show that while convective heat transfer was increased by the nanofluid, the pumping power remains the same as the base fluid (DW).

Similarly, Wen and Ding<sup>22</sup> used Al<sub>2</sub>O<sub>3</sub> 27-56 nm diameter nanoparticles in an aqueous solution to study the effects on the local heat transfer coefficient at specific locations along an axially heated pipe. The thermal conductivity of the nanofluid was measured using a KD2 thermal property meter, which uses a metrology technique based on the hot wire method. The thermal conductivity was enhanced by 10% at a volume fraction of 1.5%. For the Nusselt number calculation, the Einstein equation was used to calculate the liquid viscosity using the mean fluid temperature. Coupled with this calculation and the measurement of thermal conductivity, the Nusselt number was then calculated. At the entrance regions along the pipe, the heat transfer coefficient was found to increase by 47%. However, at downstream locations, the heat transfer coefficient is found to decay into a constant value, resulting in a 14% enhancement of the convective heat transfer coefficient compared to that for DW. The Nusselt number was found to increase with Reynolds number, and was also found to be higher for the nanofluids than for the water. The authors found that the Nusselt numbers predicted by

the Shah correlation<sup>15</sup> were not accurate and were inconsistent. The thermal conductivity enhancement of the fluid was not therefore credited as the only factor responsible for the observed enhancement of the heat transfer coefficients of the nanofluids. This enhancement, the authors propose, was attributed to particle migration, which in effect reduced the thickness of the thermal boundary layer.

Herris et al.<sup>23</sup> reported enhancements in laminar forced convection heat transfer using Al<sub>2</sub>O<sub>3</sub> (~20 nm particle size) and CuO (~50-60 nm) aqueous nanofluids. The experiment was conducted under constant temperature conditions by circulating steam through a jacket located outside a copper tube of 6 mm inner diameter and length of 1m. Density, specific heat, and thermal conductivity of the nanofluid were estimated from empirical equations, whereas the viscosity was measured using a rheometer. A 40% enhancement in heat transfer coefficient was reported for the nanofluid and was found to increase with increasing particle concentration.

In a similar study, Lai et al.<sup>24</sup> reported the enhancements of laminar forced convection heat transfer coefficients using Al<sub>2</sub>O<sub>3</sub> (~20 nm) but using a constant heat flux condition along the tube surface. The nanofluid tested was loaded with nanoparticle concentrations of 0.5%, 0.75%, and 1.0% by volume. A decrease in heat transfer coefficient was reported for an increasing axial length until the fluid reached fully developed conditions. The heat transfer coefficient was found to be enhanced by 8% for a volume fraction of 1% and by 3% for 0.5%. The enhancement is proposed to be due to the effect of Brownian convection of the nanoparticles and the interaction with the



nanoparticles and the molecules of the base fluid as well as the clustering of the nanoparticles.

The effect of nanoparticle aspect ratio was reported by Yang et al.<sup>25</sup> The effects of Reynolds number, temperature, nanoparticle concentration, nanoparticle material, and base fluid on the heat transfer coefficient enhancement in nanofluids were studied. The nanofluids were tested in a flow loop with a pipe test section of 45.7 cm length and 4.57 mm diameter. Graphite nanoparticles (20-40 nm thick, 1-2 micron diameter) with an aspect ratio of ~0.02 were suspended in two different base fluids (automatic transmission fluid, synthetic “baseoil” mixture) and two concentrations (2% and 2.5% by weight). The density, viscosity, specific heat, and thermal conductivity were experimentally measured for the conditions described above. Enhancement of thermal conductivity was reported as 56%, whereas the density and specific heat showed negligible change. Viscosity measurements were found to vary based on nanoparticle, base fluid, and nanofluid loading and a range of 10% enhancement to a 12% reduction was reported. The heat transfer coefficient was found to be enhanced by 22% for 2.5% weight concentration (50 °C) and 15% for the 2% by weight concentration (70 °C). The authors used the Sieder-Tate correlation to normalize the data as,

$$\Omega = Nu \cdot Pr^{-1/3} \left( \frac{L}{D} \right)^{1/3} \left( \frac{\mu_b}{\mu_w} \right)^{-0.14} = 1.86 Re^{1/3} \quad (3)$$

$$\Omega = a Re^b, \quad (4)$$

where  $a$ , and  $b$ , are constants used to fit the correlations to the experimental results. The values of  $a$  were higher (2-3) than the theoretical value of 1.86. The values of  $b$  were

consistent with the model ( $\sim 0.33$ ). The heat transfer coefficient enhancements between the nanofluid and base fluid were found to be 10-20% lower than the theoretical values. The effects that explain the enhancement characteristics are proposed to be the rapid alignment of nanoparticles in lower viscosity fluids that lead to less interaction between the nanoparticles and subsequent reduce heat transfer, and the depletion of nanoparticles near the wall. Ding et al.<sup>26</sup> proposed that the low aspect ratio ( $\sim 0.02$ ) of the nanoparticles could be a contributing factor for the reduced heat transfer coefficient ratios compared to the theoretical values.

### **1.6 Carbon Nanotube (CNT) Suspension**

The thermal performance of carbon nanotubes (CNT) in aqueous solutions have also been studied in forced convective heat transfer experiments. Ding et al.<sup>26</sup> presented the experimental results for convective heat transfer using CNT enhanced DW flow through a straight tube. The authors' reasons for using CNTs were the extremely high thermal conductivities, the lack of convective heat transfer analysis using CNTs, and inconsistencies observed in previous experiments using CNT nanofluids. The MWNTs were produced on a nano-catalyst from a hydrocarbon material under high pressures. Scanning Electron Microscope (SEM) and Transmission Electron Microscope (TEM) images of the MWNTs showed a high degree of entanglement and agglomeration. Surfactants sodium laurate, sodium dodecyl benzene sulfonate and gum Arabic were chosen to suspend the nanotubes and were found to stabilize the nanotubes for over one month. However, the sodium dodecyl benzene sulfonate was found to break down at high temperatures and the authors decided to use gum Arabic in the study. Nanofluid

preparation also included ultrasonication and high shear homogenization under dry conditions and dispersion respectively. The experimental setup consisted of a copper tube of length 970 mm, 4.5 mm inner diameter, and 1.85 mm thickness. Property measurements of the nanofluids included testing the thermal conductivity using a transient hot wire method and using a rheometer to measure the viscosity. The results of the study showed that viscosity decreased with increasing shear rate. The implication of increasing viscosity with increasing shear rate is that the viscosity is higher near the wall of the test section than at the core. In view of these results, the Reynolds number was calculated based on the zero-shear rate of host fluid because of the variable shear rate throughout the pipe cross section. In order to determine any effect the surfactant may have contributed to the experimental results a comparison to the base fluid with the surfactant was also presented. The enhancement of thermal conductivity was found to be 80% for a 1% weight concentration. The results of the study suggest that the convective heat transfer of the fluid is enhanced due to the enhanced static thermal conductivity, enhanced shear induced thermal conduction, decreased thermal boundary layer thickness, delayed development of the boundary layer, non-uniform shear-rate induced particle re-arrangements, and the high aspect ratios of the CNTs. A maximum enhancement of 350% compared to the base fluid was reported for a CNT concentration of 5% at a Reynolds number of 800.

## 1.7 Summary of Nanofluid Experimental Results

The results of some of the notable experimental results for nanofluids reported in the literature are summarized in Table 1. The table lists the base fluid, the nanoparticle type, the nanoparticle size, the nanoparticle concentration, and the percentage change in thermal conductivity or heat transfer coefficients.

**Table 1.** Summary of nanofluid heat transfer experiments reported in the literature.

	Author	Nanoparticle	Base Fluid	Particle Size (nm)	Volume Concentration	% Increase $\kappa_f$	$h_f$
i	Masuda <sup>27</sup> et al.	Al <sub>2</sub> O <sub>3</sub>	Water	13 DIA	4.3%	30	
ii	Eastman <sup>28</sup> et al.	Al <sub>2</sub> O <sub>3</sub> , CuO, Cu	Water, HE-200 oil	33, 36, 18 DIA	5%	60	
iii	Pak and Cho <sup>29</sup>	Al <sub>2</sub> O <sub>3</sub> , TiO <sub>2</sub>	Water	13, 26 DIA	3%		-12
iv	Wang <sup>30</sup> et al.	Al <sub>2</sub> O <sub>3</sub> , CuO	Water, EG, PO, EO	28, 23 DIA	3	12	
v	Lee <sup>20</sup> et al.	Al <sub>2</sub> O <sub>3</sub>	Water	33 DIA	4.3%	15	
vi	Eastman <sup>31</sup> et al.	CuO	Water	NA	0.9%		15
vii	Eastman <sup>8</sup> et al.	Cu	Ethylene Glycol	35 DIA	0.3%	40	
viii	Xie <sup>32, 33</sup> et al.	SiC	Water	26, 600 DIA	4.2%, 4%	15.8, 22.9	
ix	Xie <sup>34</sup> et al.	Al <sub>2</sub> O <sub>3</sub>	Water	NA	5%	23	
x	Zhou <sup>35</sup> et al.	CuO	Water	10 DIA	0.4%	17	
xi	Biercuk <sup>36</sup> et al.	SWNT	Epoxy	3-30 DIA	1% (wt.)	125	

**Table 1.** Continued.

	<b>Author</b>	<b>Nanoparticle</b>	<b>Base Fluid</b>	<b>Particle Size (nm)</b>	<b>Volume Concentration</b>	<b>% Increase</b>	
						$\kappa_1$	$h_1$
xii	Das <sup>37</sup> et al.	Al <sub>2</sub> O <sub>3</sub> , CuO	Water	38.4, 28.6 DIA		200	
xiii	Choi <sup>3</sup> et al.	MWNT	Oil	25 DIA, 50 $\mu$ m L	1%	250	
xiv	Patel <sup>38</sup> et al.	Au, Ag	Water, Toluene	10-20 DIA	0.011%	21	
xv	Xie <sup>39</sup> et al.	CNT	Organic liquid, Water	15 DIA, 30 $\mu$ m L	1%	10, 20	
xvi	Choi <sup>40</sup> et al.	SWNTs	Epoxy	20-30 (DIA) x 300 (L)	3% (wt)	300	
xvii	Xuan and Li <sup>21</sup>	Cu	Water	100 DIA	2%		39
xviii	Wen and Ding <sup>41</sup>	CNT	Water	20-60 DIA	0.8%	24, 31	
xix	Wen and Ding <sup>22</sup>	Al <sub>2</sub> O <sub>3</sub>	Water	27-56 DIA	1.6%		47
xx	Hong and Yang <sup>42</sup>	Fe	EG	10 DIA	0.55%	18	
xxi	Assael <sup>43</sup> et al.	CNT	Water	130 (DIA) x 10 $\mu$ m (L)	0.6%	34	
xxii	Wen and Ding <sup>44</sup>	TiO <sub>2</sub>	Water	30-40 DIA	0.8%	6.4	
xxiii	Liu <sup>45</sup> et al.	CNTs	ethylene glycol, engine oil	20-30 DIA	1, 2 %	12, 30	
xxiv	Murshed <sup>46</sup> et al.	TiO <sub>2</sub>	DW	10 x 40, 15 DIA	5	33,30	
xxv	Ding <sup>26</sup> et al.	MWNT	Water	25 DIA	0.5% wt	37	350

## **1.8 Project Background**

This project was sponsored by the Air Force Research Labs (AFRL) at Wright-Patterson Air Force base in Dayton, Ohio. The objective of the project was to perform a preliminary study on the efficacy of nanofluids for heat transfer enhancement and to verify if a longer, more in-depth project was justified. The interest in thermal management is driven by the increased heat flux that is projected for the onboard electronics and devices that are planned for future aircraft systems. Currently poly-alpha-olefin (PAO) is used in many of the coolant systems for onboard thermal management. However, the projections for the future technologies under development show higher heat rejection rates than can be handled by current cooling systems using PAO. The motivation of this study was to evaluate the efficacy of PAO nanofluids for enhancing the convective heat transfer in a flow loop system.

## CHAPTER II

### DESCRIPTION OF EXPERIMENTAL APPARATUS

#### 2.1 Experimental Apparatus Introduction

The experiments were performed using a flow loop apparatus that is located in the Thermal Laboratory at Wright-Patterson Air Force Base. The schematic of the experimental apparatus is shown in Figure 1 and consisted of four main components: the fin array cooler (cooling chamber), the heating block, the chiller, and the pump. Supporting instrumentation surrounded each of these main components to monitor the various properties of the system. These measurement devices included flow meters, thermocouples, and pressure transducers.

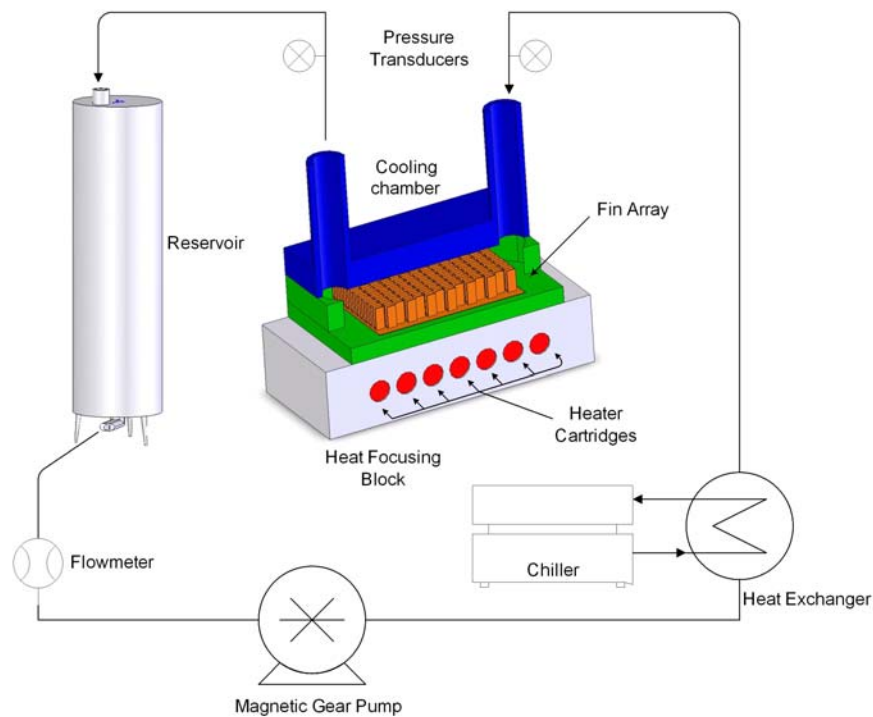


**Figure 1.** Schematic of the flow loop apparatus showing the test section (cooling chamber) with the offset fin array.

## 2.2 Flow Loop Apparatus

A heat transfer enhancement surface consisting of an offset fin array was used to heat the circulating fluid inside the cooling chamber. The fin array was made up of 14 rows of 20 fins each. The material of the fins was copper ( $\sim 400 \text{ W/mK}$ ). Copper was chosen for its high thermal conductivity. A uniform surface temperature was obtained with copper fins along with a faster response time. The fins were welded onto a copper substrate in staggered rows as shown in Figure 2. The coolant flowed perpendicular to the direction of the fins and parallel to the substrate.

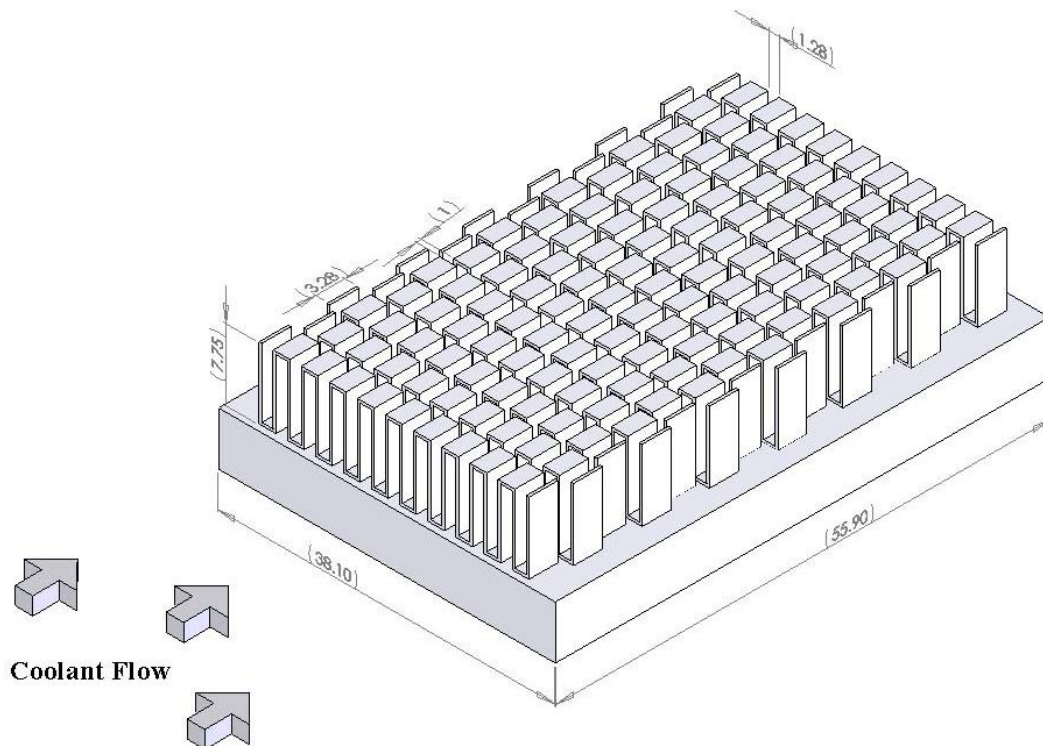


**Figure 2.** Diagram of copper fin array showing flow direction and offset fin configuration.



A thin steel plate with a width of 50.8 mm, 33.02 mm length, and a thickness of 0.5 mm was welded to the bottom of the substrate. Ten slots were cut into the steel plate at varying positions and to various depths, shown in Figure 3. Thermocouples were soldered to the substrate at the end of each slot to measure the local temperatures of the substrate. This temperature reading was then used to calculate the local surface temperatures of the copper fins.

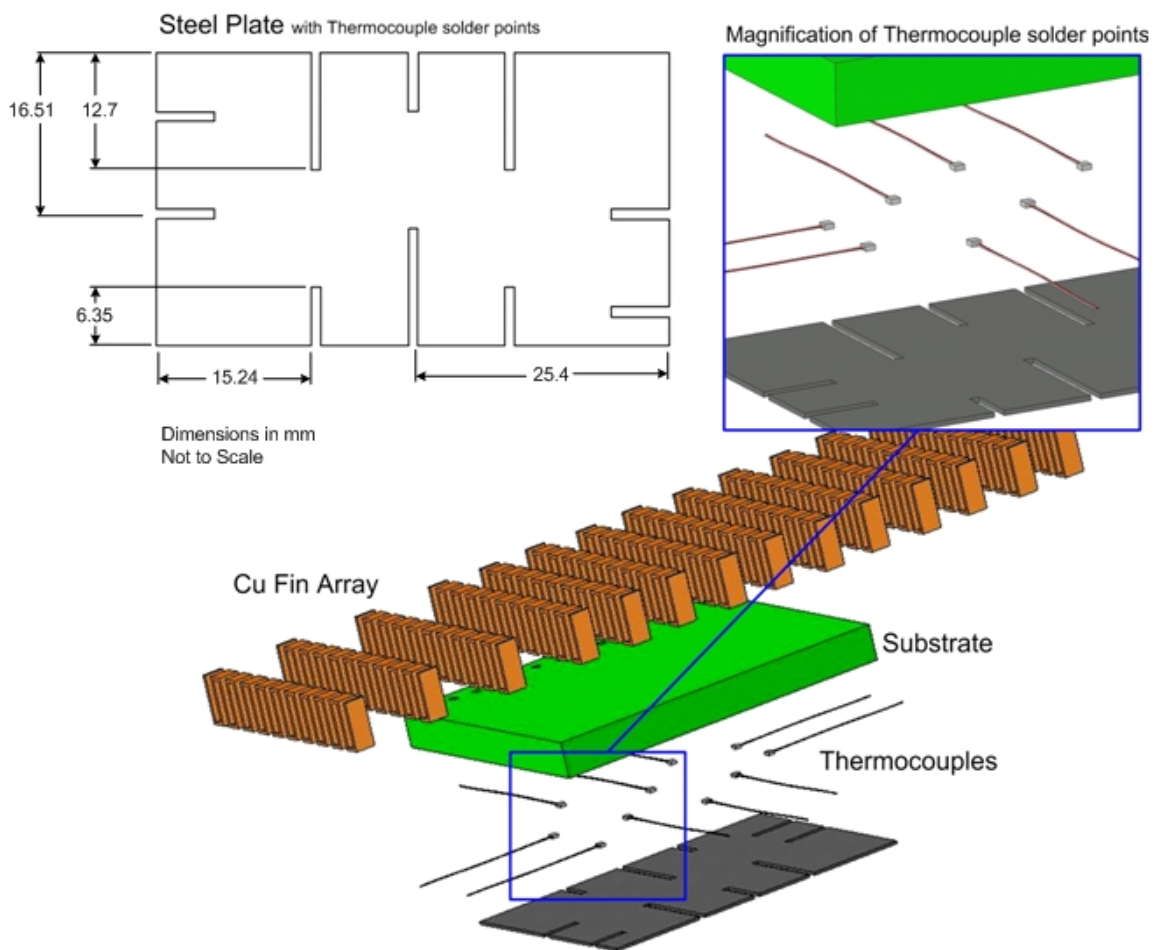


**Figure 3.** Schematic of fin array, substrate, and steel plate assembly drawing showing thermocouple placement and solder points.

The fin array was housed in a chamber with inlet and outlet ports. The flow at the inlet was directed from above the cooling chamber perpendicularly towards the substrate. A 90° change in flow direction forced the fluid flowing perpendicularly through the fins parallel to the surface of the substrate. As the fluid passed through the final row of fins, the flow was again directed at a 90° angle away from the surface of the substrate. Two rubber O-rings were used to seal the cooling chamber: one between the fin array and the fin array housing, and the other between the fin array housing and lid.

The fin array, including the substrate and thermocouple thin plate, sat atop the heat-focusing block. A thin layer of OMEGATHERM<sup>®</sup> 201 was applied between the thin plate and the heat-focusing block to reduce any contact thermal resistance between the two surfaces. The Copper block contained cartridge heaters that supplied the heat to the system. The level of heat input to the system was varied using a DC power supply where the voltage and current were monitored. A layer of FiberFrax was used as an insulator. The insulation layer minimized heat flux in the lateral direction and helped to direct the heat only in the vertical direction through the fin array. Insulation was also hand-packed around the outside of the cooling chamber and inlet and outlet ports to minimize heat.

A constant temperature water bath type chiller was used to control the temperature of the coolant before it entered the cooling chamber. The chiller apparatus had a display where the user-defined set temperature and the actual temperature of the coolant were monitored. The chiller was attached to a coil tube and shell heat exchanger. The coolant from the chiller flowed through the shell side of the heat

exchanger picking up the heat from the system fluid flowing through the tube side. The coolant temperature was set to 75° C, to be consistent with the fluid temperatures encountered on aircraft thermal management systems.

A magnetic gear pump was used to provide a minimum flow rate of 0.2 gpm (gallons per minute). For the pure PAO, maximum flow rates of up to 3 gpm could be reached, whereas, for the nanofluid the pump delivered a maximum of 2 gpm. The pump speed was adjusted via a variable voltage controller.

### 2.3 Flow Loop Instrumentation

Type-T thermocouples were placed within the cooling chamber and the heating block. The thermocouples were used to measure heat flux through the heating block and to monitor the fin surface temperatures. Thermocouples were embedded within the heat-focusing block and were arranged in two planes. Within each plane four thermocouples were placed at four locations. The placement of the thermocouples in the two planes were vertically aligned which enables the calculation of the heat flux in the vertical direction. The distance between each thermocouple in their respective pairs was measured to be 5.1 mm. The four sites in each plane were then averaged and the following equation was used to calculate the temperatures

$$T_{b,m} = T_{s,m} - \frac{qt_s}{k_s} \quad (5)$$

Thermocouples (as described in Section 2.1) monitored the temperatures on the heated side of the substrate. The type T thermocouple beads were soldered to the bare plates. The nominal diameter of the beads was 0.5 mm. The thermocouples were

soldered to the substrate at the end of each of the 0.5 mm wide slots on the thermocouple thin plate. An adhesive was then used to further secure the thermocouples within the cut slots of the thin plate and acted as further insulation of the thermocouples to ensure an accurate reading.

To measure the fluid flow rate of the system, an Omega FPD 1004 elliptical gear flow meter was used. The flow meter was operated using a Reed Switch that converted the voltage signal to a current signal between 4 mA and 20 mA. The flow rate was then monitored and recorded using a Hewlett Packard 3852A data acquisition system (DAS).

In addition to the thermocouples and flowmeter, pressure transducers were mounted at the inlet and outlet of the cooling chamber to measure the pressure drop across the fin array. The pressure readings were also monitored by the DAS.

## CHAPTER III

### EXPERIMENTAL PROCEDURE

#### 3.1 Test Parameters

The working fluids were loaded in to the flow loop apparatus using a vacuum pump. Experiments were performed by circulating the working fluids at different heating loads. Prior to loading a new working fluid into the flow loop apparatus, the previous working fluid was purged using a vacuum pump and PAO was used to flush the apparatus as well as clean any residues from the components in the flow loop.

In each experiment, measurements were performed after steady state conditions were achieved. Steady state condition was defined in these experiments to be less than 2 K change per hour. The thermocouples attached to the heated side of the substrate were monitored and used as the basis for the steady state measurements. Each test was run at a predetermined flow rate that was maintained constant throughout the entire test. As discussed in Section 2.3, the range of flow rates attainable by the magnetic gear pump was the limiting parameter in the experiments. In addition to maintaining the flow rate at a constant value, the entrance temperature of the fluid was also kept constant at a predetermined value. The inlet temperature was maintained at a constant value by the automated temperature control apparatus on the chiller. The inlet temperature to cooling chamber for the working fluid was held at a constant value of 75 °C for all experiments. This value of inlet temperature was chosen to conform to the typical operating conditions on aircraft thermal management systems that utilize PAO as the cooling fluid.

### 3.2 Data Collection

The entire testing procedure was automated using a Visual Basic program that controlled the power supply, and monitored the DAS system. The chiller and pump were controlled independently from the Visual Basic software. After reaching steady state, the input power to the system was incremented by a pre-determined margin. The supply power was stepped up by 100 W increments during the experiments. As the system reached steady state at each power input (0 W, 100 W, 200 W, 300W, 400W, and 500 W), the software averaged and recorded five sets of data at fifteen second intervals. The time-averaged readings were used to assess the transient and steady state data for a given power input as well as to verify if steady state conditions were reached. After recording was completed on reaching steady state conditions, the input power was again ramped up an additional 100 W from the previous stage. A limit of 500 W was set for the experiments to ensure that the PAO and PAO nanofluid were not exposed to temperatures exceeding the maximum allowable temperature. The maximum allowable temperature of PAO was listed to be 166 °C by the manufacturer data sheet, as referenced in Appendix I. Also, the data for the maximum allowable temperature of the nanofluid was not available at the time of the experiments. Therefore, using a conservative approach, the system was set to cut off the input power if the fin surface temperature ever reached 150° C for both the PAO and the nanofluid PAO. Only at very slow flow rates (< 0.3 gpm) did our testing ever encounter high enough temperatures to trip the cut-off point of the input power. At the conclusion of each test, the fluid was circulated with the power input switched off until a fin surface temperature of less than

75° C was reached. This was performed to ensure that residual heating effects would not degrade the working fluid or affect the subsequent experiments. As a system steady state took close to one hour for each stage, a maximum of two test runs could be completed in a one-day time span, while typically one test run would be performed in one day.

### **3.3 System Flushing Procedure**

During the testing of both the pure PAO and the PAO nanofluid, it was necessary to evacuate the test loop in order to nullify any residual effects of the previous tests. After testing with the nanofluid, it was observed that the agglomerated nanoparticles remained on the surface of the fin array. Since the study's primary focus was to compare the heat transfer effects of the nanoparticles deposited on the fin surface, a clean fin array at the start of each test was important to ensure the reliability of the data. A system flush was therefore performed after each test with the nanoparticle solution. The system flush was performed to clear the fin surface of any precipitated nanoparticles. Pure PAO was used as the medium to flush the system. While flushing the flow loop, the flow loop was opened at the suction line of the pump. A reservoir with clean PAO was attached to the suction line of the pump, and a waste reservoir was connected to the open end of the flow loop. This way fresh PAO was completely circulated through the system once and then pumped into the waste reservoir. The flow rate was varied and then run at close to peak flow rates to clean out the cooling chamber and the flow lines of any remaining nanoparticles. This flushing procedure was continued until the flushed PAO appeared unaltered in color (similar to the pure PAO).

### 3.4 Measurement Uncertainty

The uncertainty of the experimental data depends on the uncertainties of the temperature readings, flow rate readings, and the data acquisition system. For the testing of the baseline results, thermal properties are included in the analysis. The thermal property values used were based on published correlations using the average temperature of the inlet and outlet of the test section.

In order to calculate the uncertainty of the experimental data, the uncertainties of the temperature measurements, flow rate measurements, and the data acquisition system were determined. The temperature readings involved two sources of measurement error, i.e., the physical location, and the accuracy of the thermocouples. The accuracy of the positioning between two thermocouples was  $\pm 0.3$  mm based on the machining procedure. The second area of uncertainty lies within the construction and characteristics of the type of thermocouple chosen. The accuracy of the thermocouple measurements were reported to be  $\pm 0.2^\circ$  C.

The flow rate measurement was obtained from the OMEGA positive displacement elliptical gear flow meter. The flow meter measurement utilized a Reed sensor and then transmitted the 4-20 mA signal to the data acquisition system. Since the flow meter reading was independent of viscosity of the fluid, a calibration procedure using water was sufficient for ensuring the accuracy of the measurements. The calibration procedure for the flowmeter involved timing the flow rate of water through the flow meter at a constant flow rate. The flow meter measurement was found to have



no bias and was within  $\pm 1\%$  of the calibrated values. The manufacturer data sheet reported the error of flow measurement to be  $6.3 \times 10^{-4}$  L/s.

The data acquisition system (DAS) was a Hewlett Packard 3852A and was used to record the experimental parameters of the test. Since the DAS had 8-bit recording capability the accuracy of the temperature readings was reported as  $\pm 0.02^\circ$  C. The measurements were performed at a frequency of 50 times per minute and were recorded by a computer.

## CHAPTER IV

### NANOFLUID CHARACTERIZATION

#### 4.1 Nanoparticle and Nanofluid Manufacture

As discussed in Section 1.2 a nanofluid consists of nanoparticles dispersed in a base fluid. In the experiments using the flow loop, the performance of PAO was compared to the nanofluid. PAO is used in the cooling of onboard aircraft electronics, devices and equipment. Hence, PAO was chosen as the base fluid in the experiments. The nanoparticles used in the study were manufactured by Dr. K. Lafdi of the University of Dayton Research Institute in Dayton, Ohio. Exfoliated graphite nanoparticles of 20  $\mu\text{m}$  in diameter and 100 nm in thickness were used in this study. Seventeen grams of the nanoparticles obtained from Dr. Lafdi were added to 1200 grams of PAO, yielding a weight concentration of 0.6%. A second nanofluid solution was obtained by diluting the nanofluid by an equal weight of PAO to yield a weight concentration of 0.3%.

#### 4.2 SEM Analysis

After testing the 0.6% by weight concentration of the nanofluid in the cooling flow loop, a small section of the fin array was removed from the test section and a SEM was used to study the surface. In Figure 4, the arrows show the three distinct nanoparticles that precipitated on the fin surface. The nanoparticles appear translucent to the incident electron beams. Hence, in the SEM images the precipitated nanoparticles appear translucent. The nominal diameter of the nanoparticles at the beginning of the

experiment was 20  $\mu\text{m}$ . In the SEM images at the end of the experiment the nanoparticles were smaller in size than in the stock solution probably due to attrition and abrasion.

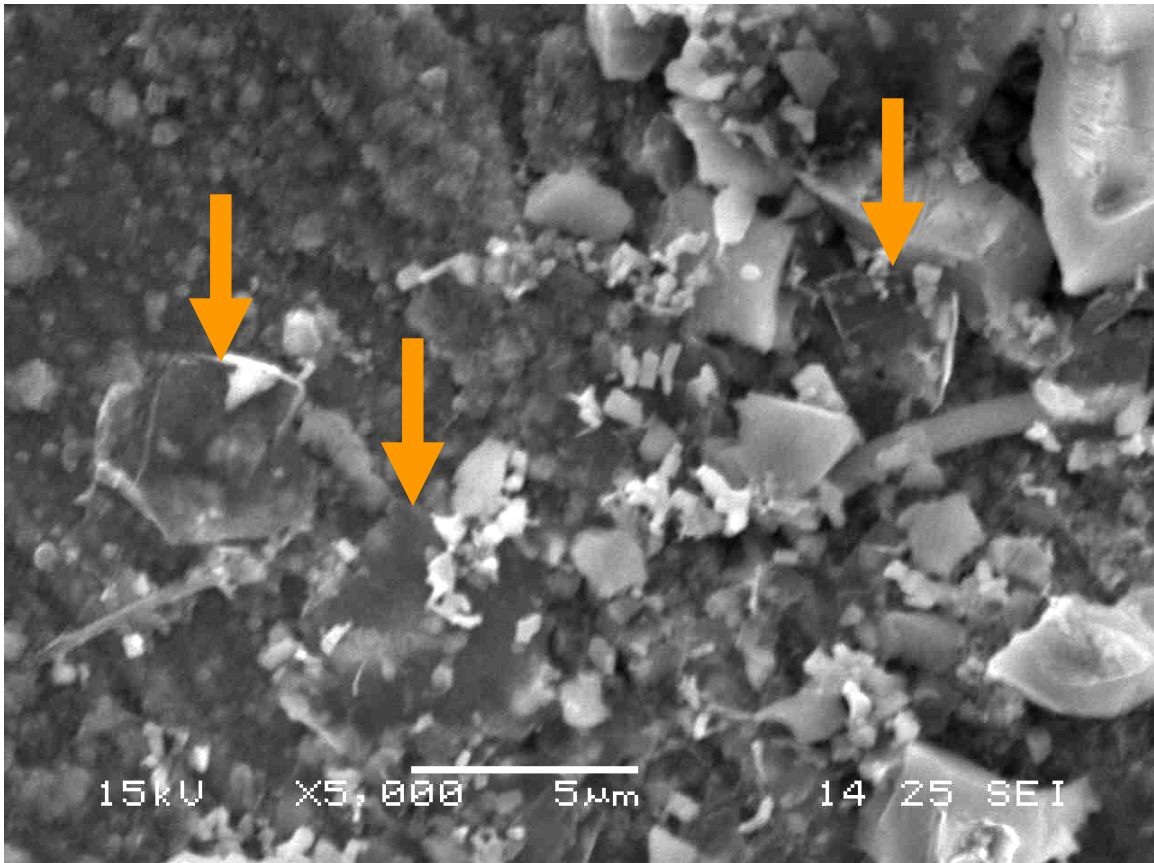


**Figure 4.** Scanning Electron Microscopy (SEM) image showing precipitated nanoparticles. The exfoliated graphite nanoparticles appear semi-transparent in the image and are indicated by superposed arrows in the image.

Figure 5 shows agglomeration of nanoparticles on a copper surface. The graphite flakes precipitate on the surface of the copper. As will be discussed in Section 5.3, the nanoparticles agglomerated on the surface of the copper may act as nanofins, creating a less resistive path for thermal energy to travel from the copper fins to the cooling fluid.

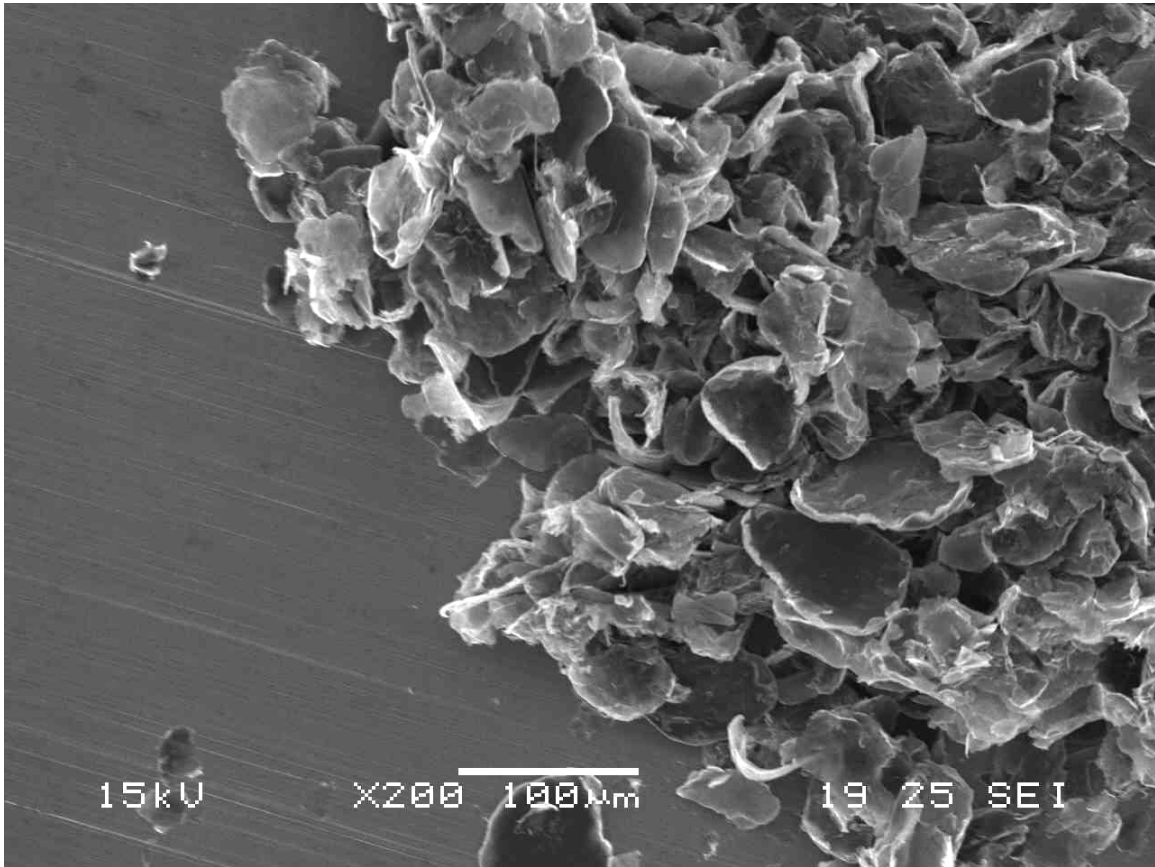


**Figure 5.** Scanning Electron Microscopy (SEM) image showing surface agglomeration of the precipitated exfoliated graphite nanoparticles that were deposited on the fin surface.

### 4.3 EDX Analysis

Energy Dispersive X-Ray (EDX) analysis was performed on the fin surface to gain further insight into the precipitation on the fin surface. EDX is a type of spectroscopy that is used to uniquely identify individual elements in the periodic table based on the unique spectra emitted by each element when excited by electromagnetic waves. In the EDX instrument the incident beam is absorbed and emitted by the atoms of the test sample. Each individual element emits characteristic spectral lines that are

detected and converted into voltages. The voltage variations are analyzed and the quantity of each voltage signal (count) is plotted. Based on the count and voltage output, the elements present are identified and the relative amounts of each element are quantified. Figure 6 shows the peaks of both Carbon and Copper from the EDX spectra for the deposited nanoparticles on the copper fin surface. This supports the hypothesis of nanoparticle precipitation on the fin surface acting as nanofins.

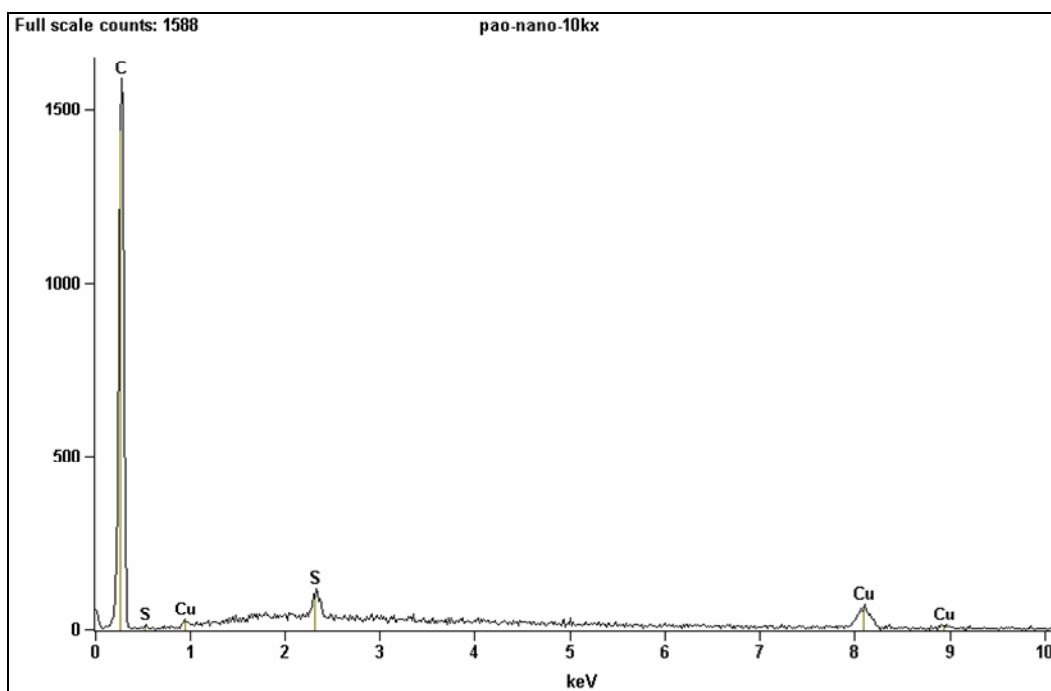


**Figure 6.** EDX (Energy Dispersive X-Ray) spectra of copper (Cu) fin surface performed after the experiments showing elemental surface deposition of carbon (C).

## CHAPTER V

### RESULTS AND DISCUSSION

#### 5.1 Thermal Property Analysis

An important aspect of this study was to assess the thermal property effects with the addition of nanoparticles to the base fluid. To gain a complete understanding of the thermal property effects, the thermal diffusivity, viscosity, density, and specific heat of the nanofluid were measured.

##### 5.1.1 Viscosity Measurements

The rheological data shown in Figure 7 compares the variation of viscosity with temperature for PAO and nanofluid (0.6% concentration by weight). The tests were carried out using a concentric cylinder shear measurement apparatus and by varying the temperature of the sample. The viscosity of PAO is observed to decrease with an increase in temperature. The nanofluid viscosity in contrast has an opposite trend. As the temperature of the nanofluid is increased, no appreciable change in viscosity is seen over the baseline until the nanofluid reaches a temperature of  $\sim 100$  °C. At this temperature, the viscosity begins to increase rapidly. The data suggests that the nanofluid coagulates at temperatures above 100 °C. In addition, the absolute value of the nanofluid viscosity is close to two orders of magnitude larger than the PAO.

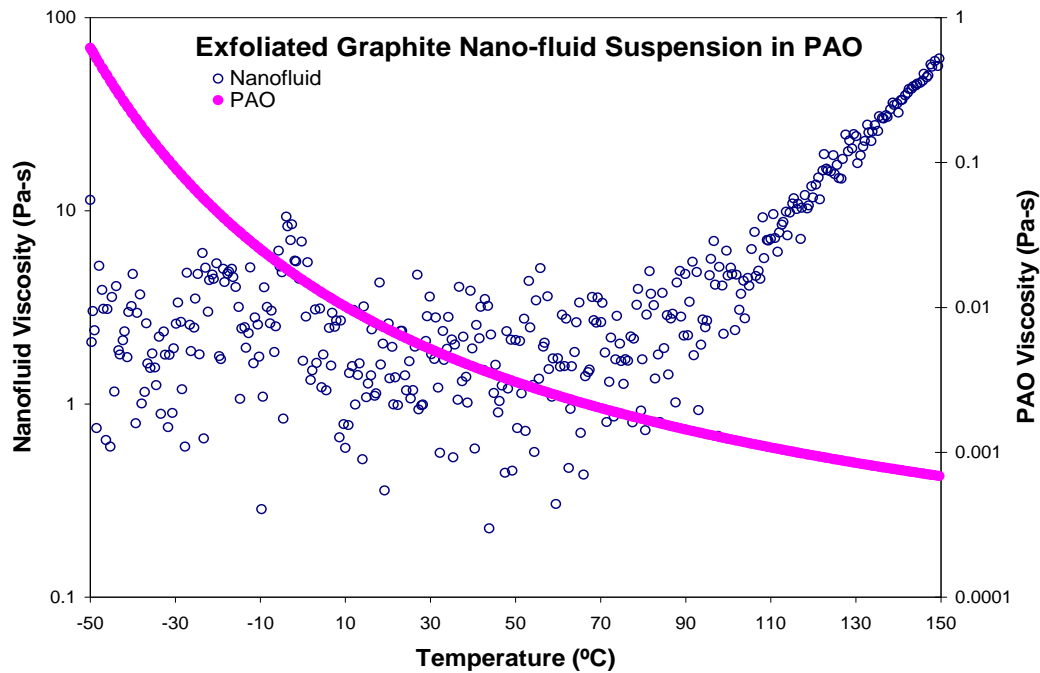
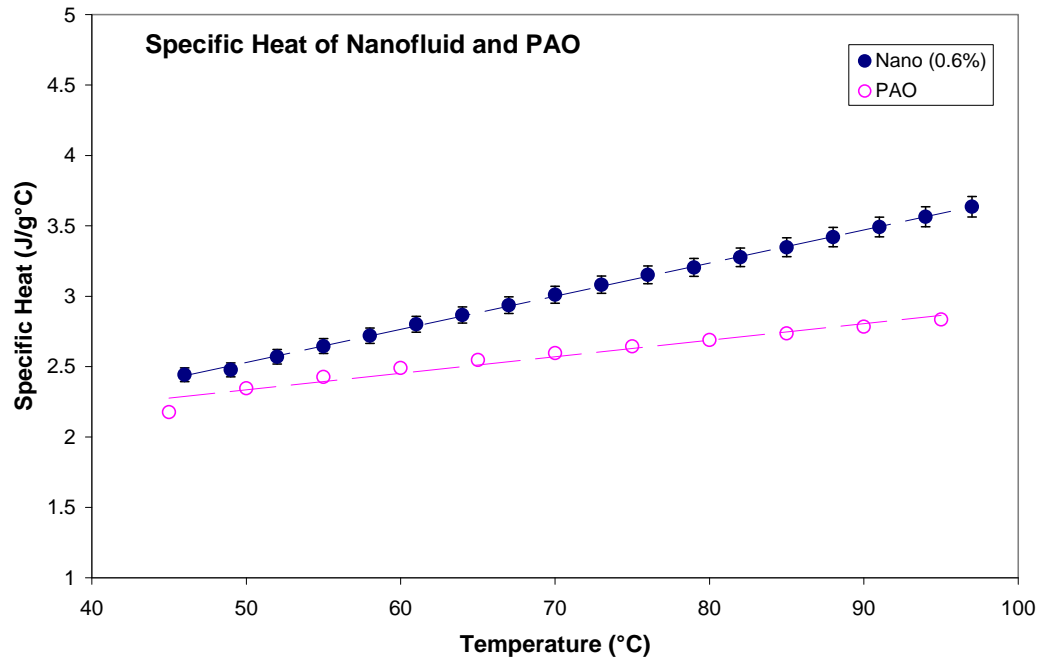


Figure 7. Viscosity measurements for PAO and nanofluid (0.6% concentration by weight).

### 5.1.2 Specific Heat Measurements

The specific heat of the two fluids were also tested and compared. The specific heat of PAO nanofluid and PAO were obtained by using a Differential Scanning Calorimeter (DSC) to measure the specific heats of the fluids. The specific heat was measured at different temperatures and the results are presented in Figure 8 below with an accuracy of  $\pm 2\%$  as reported by the manufacturer. A comparison of the nanofluid to the base PAO shows an enhancement by as much as  $\sim 50\%$ .



**Figure 8.** Specific heat measurements for PAO and nanofluid (0.6% concentration by weight).

### 5.1.3 Density Measurements

A simple density measurement was used to quantify the density change with the addition of the nanoparticles. Since the published data for PAO<sup>47</sup> showed only small changes in density with temperature change, the density measurement was taken only at room temperature and assumed not to change with a varying temperature. By measuring the weight and volume of a sample of the nanofluid, the density was calculated. A fixed volume of the sample of nanofluid was extracted from the reserve using a syringe and the mass of the sample was measured with a digital scale. The measurement was repeated five times to validate the accuracy of the method. In addition to the viscosity,



density, and specific heat of the fluids, the thermal diffusivity of the fluids was measured.

#### **5.1.4 Thermal Diffusivity Measurements and Thermal Conductivity**

Figure 9 shows the enhancement of thermal diffusivity for the PAO nanofluid. Thermal diffusivity was not measured for the pure PAO. Measurements were taken with a Laser Flash Apparatus (LDA 447) for the nanofluid solution of 0.6% concentration with an accuracy of  $\pm 5\%$  as reported by the manufacturer. The results for pure PAO plotted below are taken from a correlation of thermal conductivity in published work. The thermal diffusivity was then calculated by Equation 6 with the published density data, and experimental specific heat data. As the thermal conductivity (Figure 10) of the correlations for pure PAO show a negligible change with variation in temperature, a similar result is shown in the thermal diffusivity.

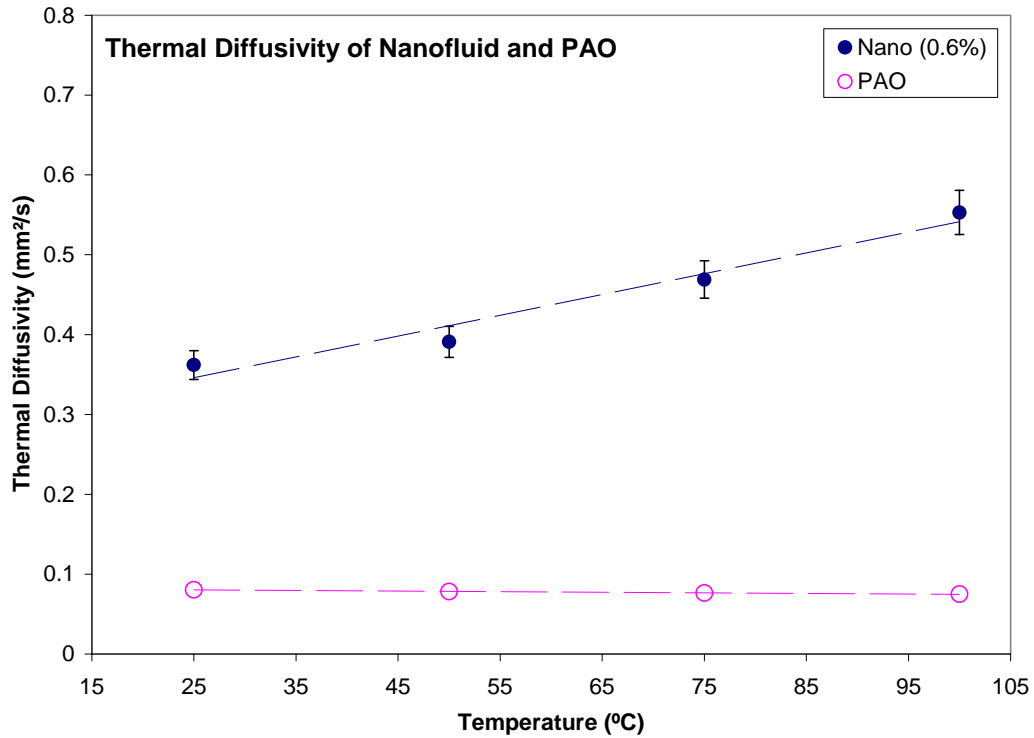


**Figure 9.** Thermal diffusivity measurements for PAO and nanofluid (0.6% concentration by weight).

With these thermal property measurements, we determined the thermal conductivity of the nanofluid based on the relation:

$$\alpha_l = \frac{k_l}{\rho_l c_{p,l}} \quad (6)$$

Figure 10 shows the results of the thermal conductivity calculations. The thermal conductivity calculations are based on the thermal diffusivity, density, and specific heat of the nanofluid, and the corresponding pure PAO points from a published correlation<sup>47</sup>. The figure shows that the thermal conductivity of the nanofluid increases with increase in temperature. This trend is similar to that observed for the thermal diffusivity of the nanofluid.

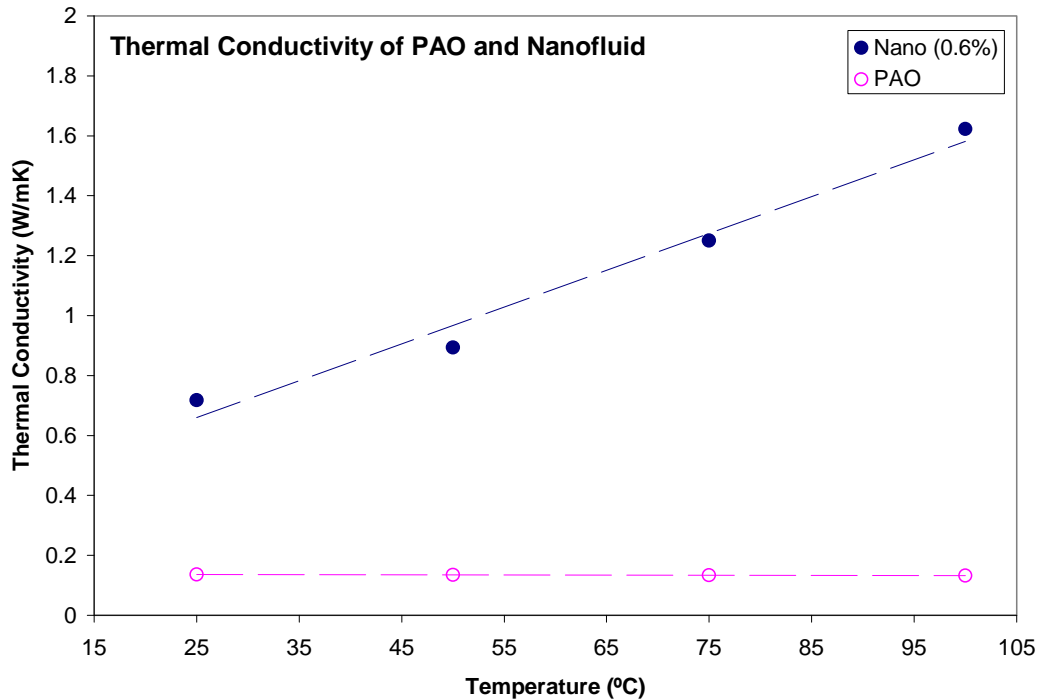


**Figure 10.** Thermal conductivity measurements for PAO and nanofluid (0.6% concentration by weight).

The results presented above show that the thermal properties of PAO are enhanced due to the addition of nanoparticles. Data reported in literature show that the conventional models for solid-liquid dispersions do not accurately predict results for thermal property enhancements. The results from this study indicate similar disparities in the thermal properties when compared to the conventional models.

## 5.2 Baseline Test Results

To validate and establish a baseline for the experiments, experiments were performed initially using PAO in the flow loop. The experimental data was found to be consistent with previous results reported in the literature (e.g., Lin et al<sup>48</sup>). Experiments were performed using PAO as the working fluid and an offset fin array. The results were

consistent with the correlation published by Weiting<sup>49</sup>. These results and comparison with Weiting's correlation<sup>49</sup> are presented in Figure 11 below. The  $Nu/Pr^{1/3}$  is plotted as a function of the Reynolds number (Re) for the various flow rates of PAO. The Nusselt number, Nu, was calculated by first calculating the heat transfer coefficient of the fin-liquid interface. The heat transfer coefficient was iteratively calculated from the implicit equation,

$$Q = \left\{ n_f n_{st} \sqrt{h P k_f A_c} \tanh(ml_1) + A_b h \right\} (T_{b,m} - T_{l,m}), \quad (7)$$

where,

$$m = \sqrt{\frac{hP}{k_f A_c}}. \quad (8)$$

The experimental results were found to be consistent with results reported by Lin et al. and the Weiting's correlation<sup>49</sup> which are expressed as,

$$Nu = 0.483 \left( \frac{l}{D_h} \right)^{-0.162} \left( \frac{b}{a} \right)^{-0.184} Re^{0.464} Pr^{1/3}, \quad (9)$$

where,

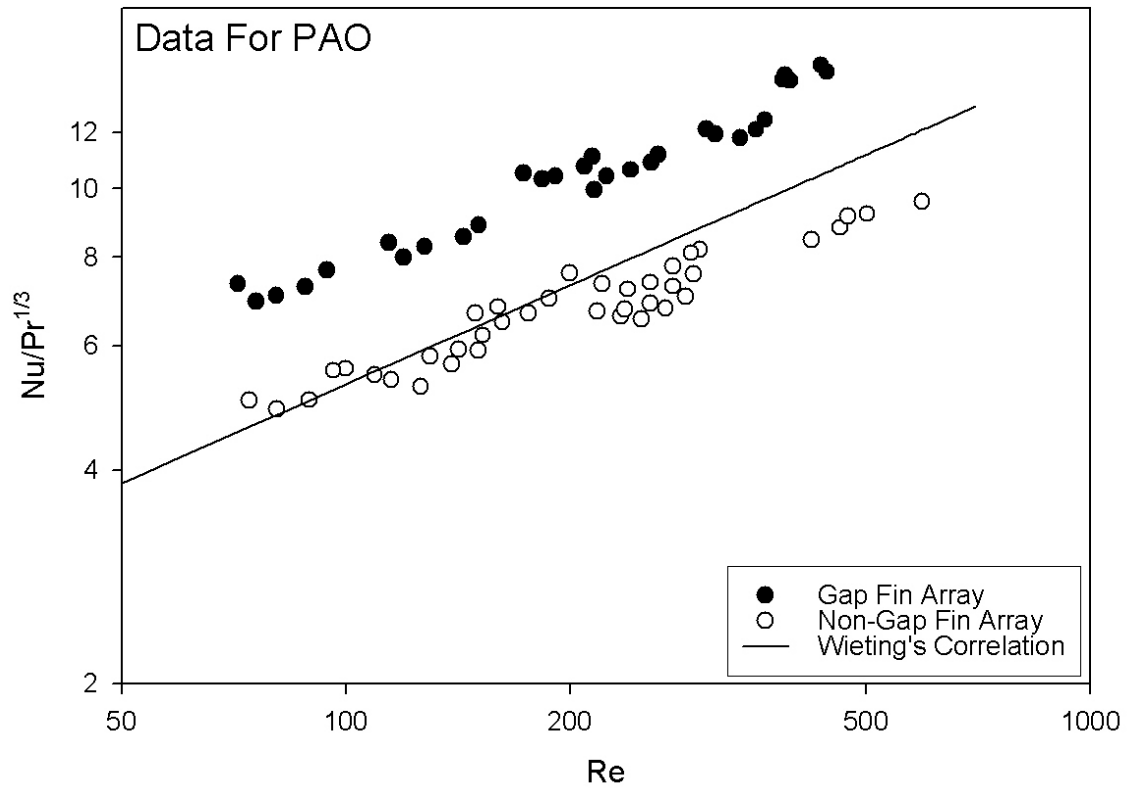
$$Nu = \frac{h D_h}{k_l} \quad (10)$$

$$Re = \frac{\rho u D_h}{\mu} \quad (11)$$

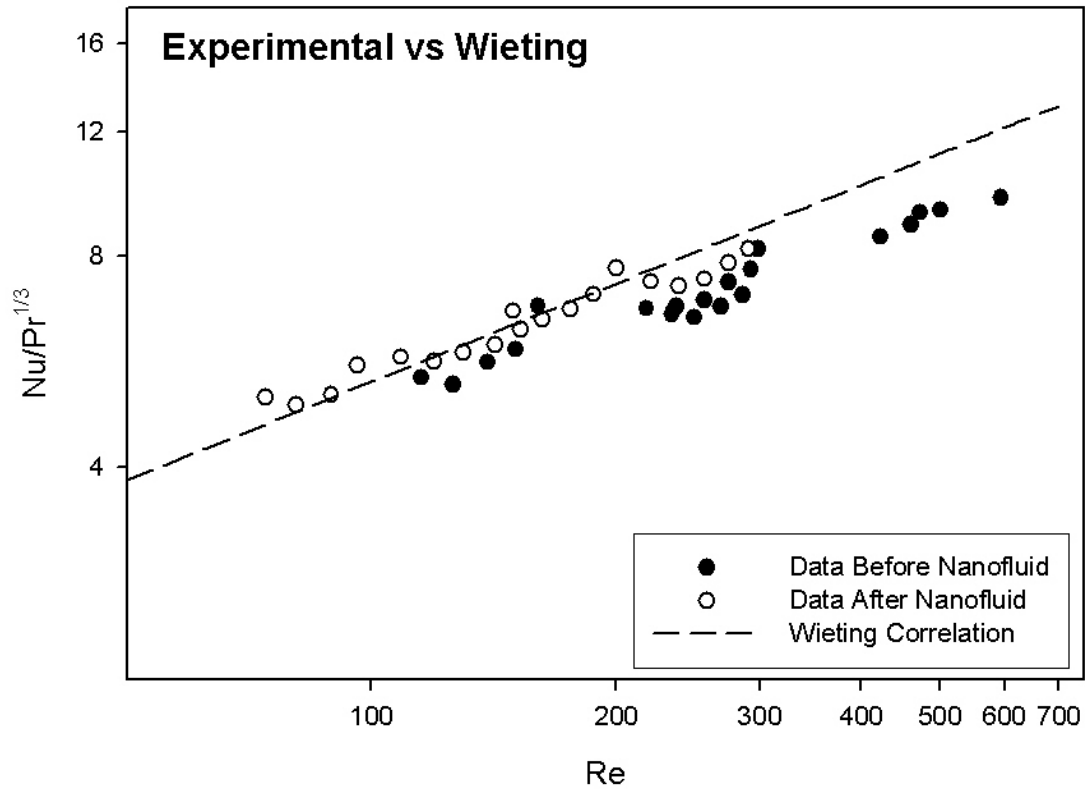
$$D_h = \frac{2ab}{(a+b)}. \quad (12)$$

Figure 11 shows the plot of  $Nu/Pr^{1/3}$  vs. the Reynolds number for the two configurations of the fin array used in original testing by Lin et al.<sup>48</sup> The gap fin array test results were used exclusively for the comparison of the pure PAO to the nanofluid. In subsequent experiments the non-gap fin array was used by flowing PAO to study the heat transfer through the fin array after the system had been introduced to nanofluid. In Figure 12, the non-gap fin array results are shown to directly compare with the Weiting correlation. In Weiting's published data<sup>49</sup>, a non-gap fin array was used to develop the correlation. In addition, the gap fin array data was found to be consistent with the data reported by Lin et al.<sup>48</sup> The gap fin array data follows the trend of the Weiting correlation<sup>49</sup> after the heat transfer enhancement was adjusted by ~20%.

In Figure 12, the results of testing with the non-gap fin array are shown for the before and after cases of nanofluid testing. In order to study any residual effects of the nanoparticles on an evacuated system, the results show a negligible difference in the measured heat flux both before nanofluids were used and after nanofluids were used, followed by experiments that were performed after flushing the flow loop apparatus with pure PAO. These results verified that the flushing procedure described in Section 3.3 adequately removed any nanoparticles from the flow loop apparatus that would have affected the forced convective heat transfer.



**Figure 11.** Variation of  $Nu/Pr^{1/3}$  with Reynolds number for flow through both gap-fin and non-gap offset fin array. Weiting's correlation<sup>49</sup> is plotted for comparison with the experimental data.



**Figure 12.** Variation of  $Nu/Pr^{1/3}$  with Reynolds number using PAO for the experimental apparatus before being exposed to the nanofluid and after exposure to the nanofluid.

The results of the baseline tests demonstrated the validity of the experiments to quantify the effects of nanoparticles/ nanofluids on the performance of the flow loop apparatus for cooling. Because the baseline data collected agrees closely with the published data of Lin et al.<sup>48</sup>, any change in system performance can be attributed to the addition of the nanoparticles/ nanofluids.

### 5.3 Nanofluid Test Results

The test procedure described in Chapter III was followed and the results are presented below. Figure 13 shows the experimental results for an input power setting of 300 W for PAO and nanofluids (at 0.3% and 0.6% concentration of nanoparticles by weight). At this heat input, a consistent enhancement of approximately 4% was observed at the different flow rates for 0.3% by concentration nanofluid as compared to pure PAO. However, for the 0.6% by weight concentration of the nanofluid, the enhancement is doubled to 8%.

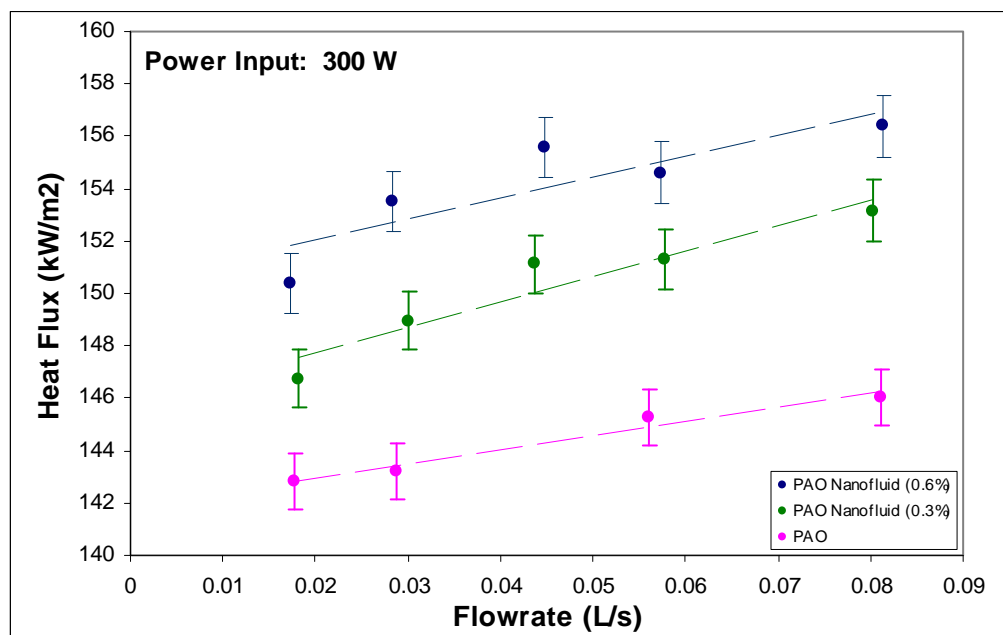


**Figure 13.** Heat flux as a function of flow rate for both nanofluid concentrations and pure PAO for a heat input of 300 W.

The observed trends at an input power setting 400 W (Figure 14) are similar to the behavior of the cooling system at an input power of 300 W: An average enhancement of 4% for the 0.3% by weight concentration nanofluid, and an average



enhancement of 7% for the 0.6% by weight concentration nanofluid is observed at an input power setting of 400W. For each flow rate the experiments were repeated at least twice to verify repeatability of the experiments. For each flow rate, the variance in heat flux for a specific fluid was below 1% for the repeated tests.

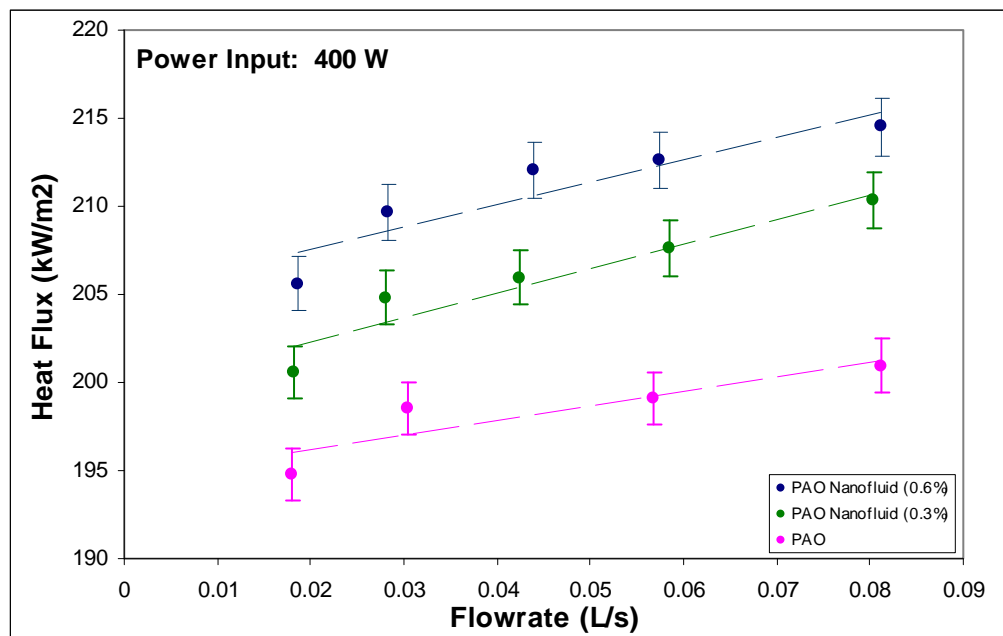


**Figure 14.** Heat flux as a function of flow rate for both nanofluid concentrations and pure PAO for a heat input of 400 W.

Similarly, experiments were performed at an input power setting of 500W and the results are plotted in Figure 15. In Figure 15 it is observed that the results for 500W show a marked deviation from the results obtained for lower input power. At low flow rates the heat flux for the nanofluid (0.3% concentration) is almost identical to the heat flux for PAO. At higher flow rates an enhancement of less than 3% is observed for the same nanofluid. At higher nanoparticle concentration (0.6% by weight concentration nanofluid) only 8% heat flux enhancement is observed compared to PAO for low flow rates. At higher nanoparticle concentration an anomalous increase in heat flux is

observed with flow rate for low flow rate. This anomalous increase at low flow rates is found to subsequently decrease or marginally increase as the flow rate is increased. For higher flow rates ~5% heat flux enhancement was observed compared to PAO. These anomalous results can be explained by relating the viscosity of the nanofluid to the local surface temperatures on the fins.

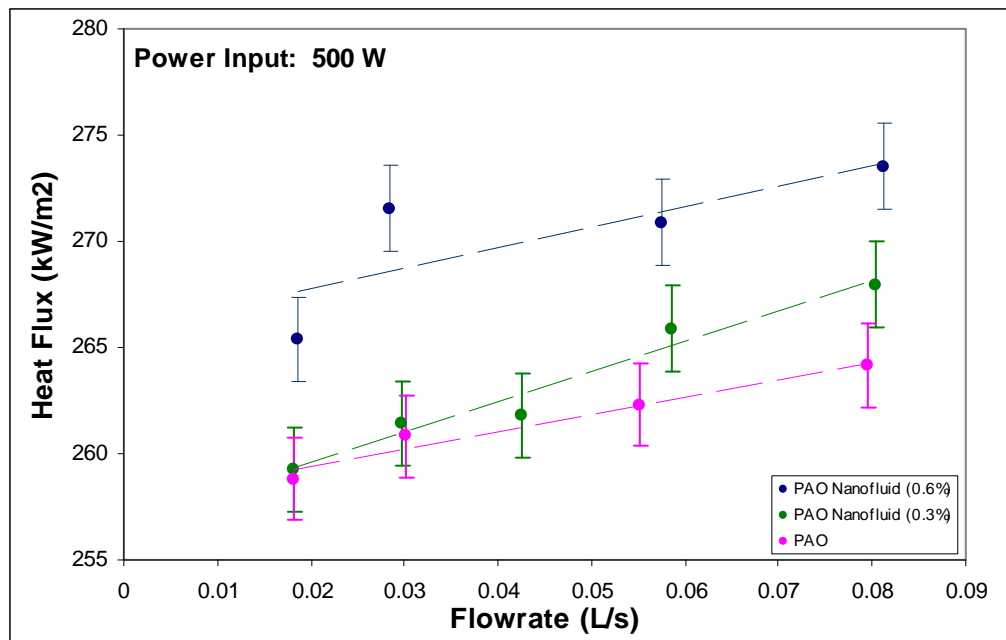


**Figure 15.** Heat flux as a function of flow rate for both nanofluid concentrations and pure PAO for a heat input of 500 W.

The enhancement of the heat transfer through the fin array at low input power (300W and 400W) can be explained due to the formation of enhanced heat transfer surfaces (“*nano-fins*”) formed by the deposited nanoparticles on the copper fin surface. As was presented in Section 4.3, EDX and SEM analysis show that nanoparticles were deposited on the copper surface. The deposited nanoparticles act as high aspect ratio fins (*nano-fins*) that create a potentially lower thermal resistance path. This provides an

additional transport mechanism for the total heat flux which is absent for PAO. The increased surface area provides a much larger solid particle-to-liquid area for conduction heat transfer into the nanofluid. A fluid with a higher concentration of nanoparticles will necessarily produce more nanofins on the heat transfer surface, thereby increasing further the enhancement through the heat transfer surface. However, the pool boiling heat flux data in the literature indicates that at a certain threshold value of the nanoparticle concentration the formation of the nanofins can actually lead to fouling of the surface resulting in decrease in heat transfer. The experimental data reported here shows that such a threshold nanoparticle concentration is larger than 0.6% concentration by weight.

As discussed in Section 5.1.1, the viscosity of the nanofluid increases rapidly at a threshold temperature of 100 °C, probably due to coagulation of the nanofluid. The coagulation of the nanofluid may contribute to the decrease in heat flux enhancement and anomalous behavior observed at low flow velocities for experiments performed at input power of 500W. At low flow velocities the residence time of the fluid volume is higher resulting in higher local temperatures of the fluid in contact with the fin surface. Higher local temperatures can potentially cause coagulation of the nanofluids on the fins resulting in higher pressure drop and lower heat fluxes. Also, the coagulation of nanofluids could result in agglomeration of multiple nanoparticles resulting in larger particles. The surface area to volume ratio of the nanoparticles would decrease drastically in such an agglomeration process. Such a temperature dependent process of coagulation and agglomeration can be reversible or irreversible. In addition, the surface

precipitation of the particles on the heater surface (formation of “nano-fins”) could also be modified reducing their efficacy. Since the nanofins are essentially the low resistivity bridge between the copper fins and the bulk fluid (PAO), the enhancement is expected to decrease as the nanofin formation is depleted.

#### **5.4 Nanofluid Test Analysis**

The PAO and 0.6 % by weight concentration PAO nanofluid were compared based on the flow velocity. The large difference in viscosity between the PAO and PAO nanofluid caused the data for each fluid to agglomerate to high and low Reynolds numbers respectively – effectively preventing a common basis for comparison based on Reynolds number. In Figure 16 a form similar to the Weiting correlation is used to compare the heat transfer characteristics of the two fluids based on similar flow velocities. As shown in Figure 16 - for the 300 W input, the PAO nanofluid consistently has a higher correlation constant than for the PAO for the same flow rate. This agrees with the results discussed in Section 5.3.

Similar plots are shown in Figure 17 and Figure 18 for the experiments conducted for heat inputs of 400 W and 500 W, respectively. The results and trends in these figures are in good agreement with Figure 16.

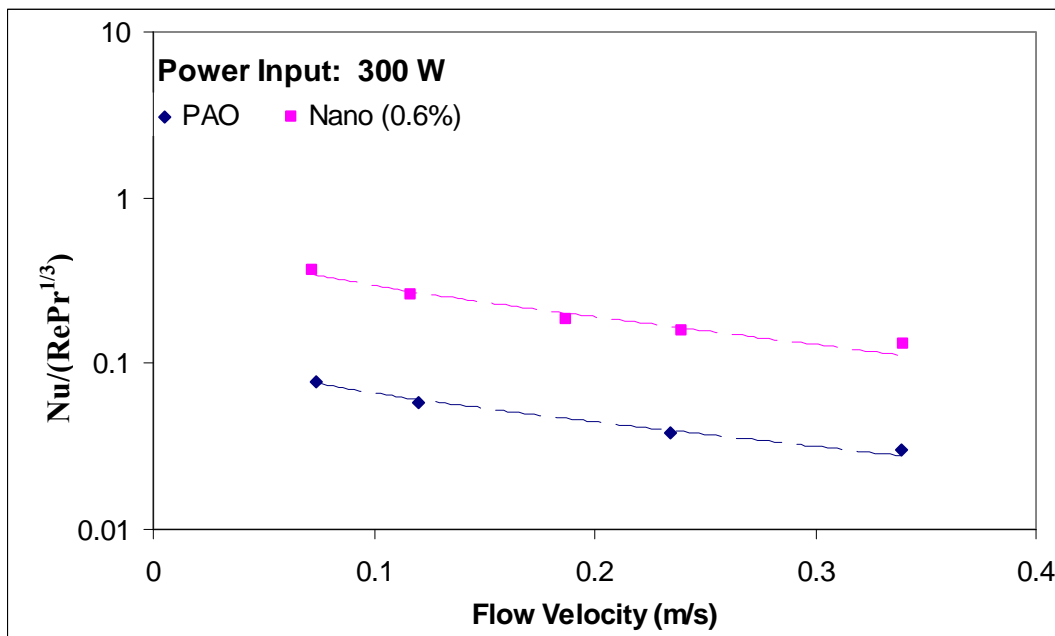


**Figure 16.** Comparison of PAO to 0.6% PAO nanofluid using Weiting correlation at 300W input.

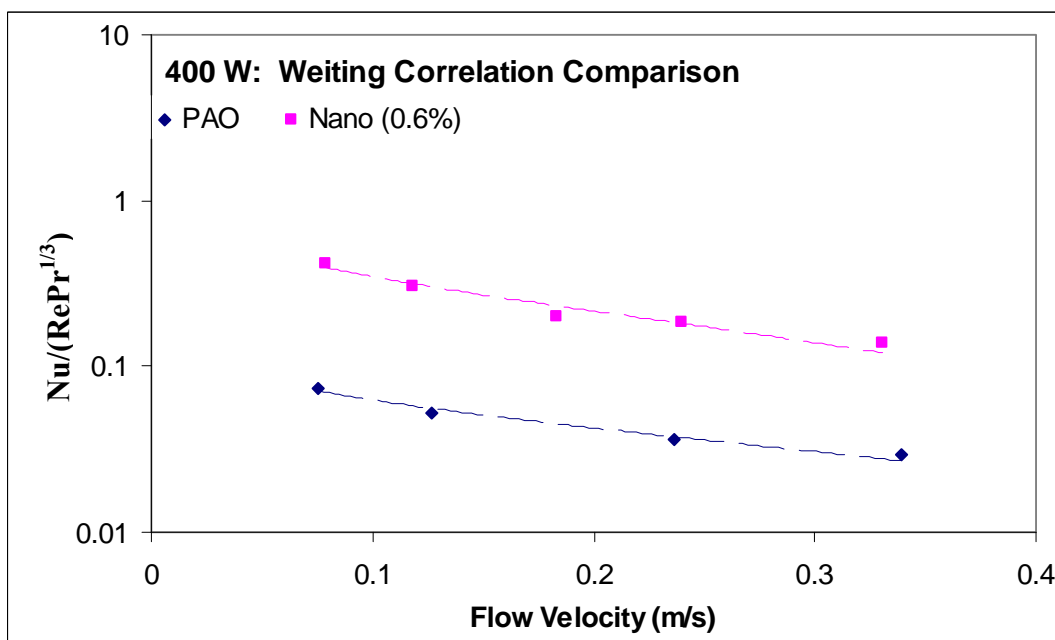


**Figure 17.** Comparison of PAO to 0.6% PAO nanofluid using Weiting correlation at 400W input.

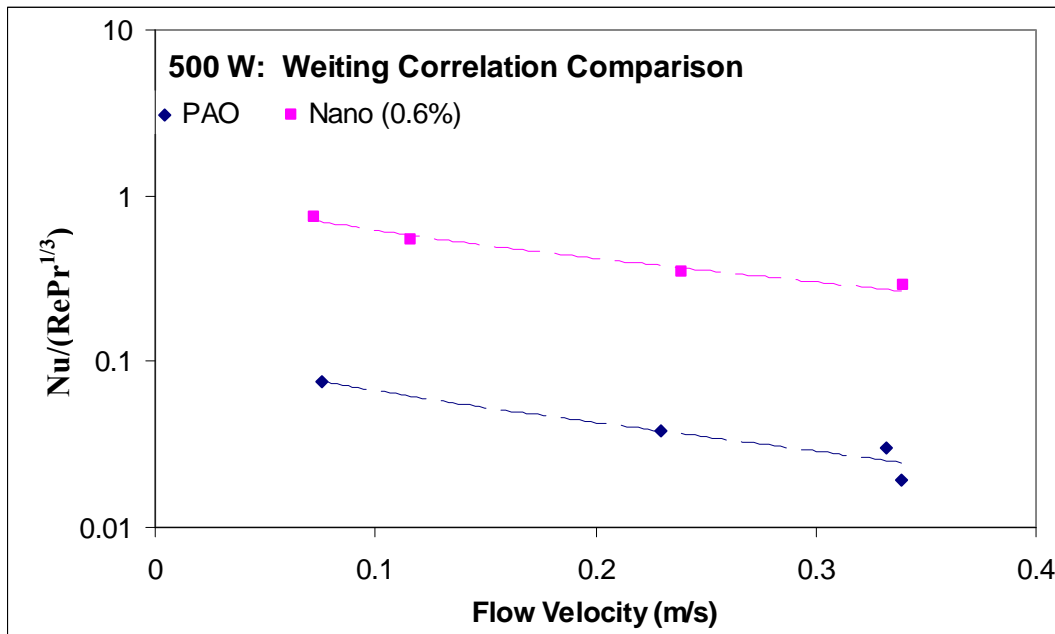


**Figure 18.** Comparison of PAO to 0.6% PAO nanofluid using Weiting correlation at 500W input.

A direct comparison between the Nusselt numbers and the Weiting correlation relationship between the Reynolds and Prandtl number is shown in Figures 19-21 for the 300 W, 400 W, and 500 W, respectively. The trend lines (best fit line) in Figures 19 and 20 (for heat input of 300 W and 400 W, respectively) have less variability than for Figure 21. As discussed in Section 5.3, the anomalous behavior at 500 W input power can be attributed to the coagulation of the nanofluid at higher temperatures that occur at higher heat input. The results used in Figures 19-21 are tabulated in Table 2, Table 3, and Table 4. The average enhancement of the correlation coefficient is approximately 4 times for the 300 W and 5 times for 400 W heat input experiments, for the nanofluid compared to PAO.

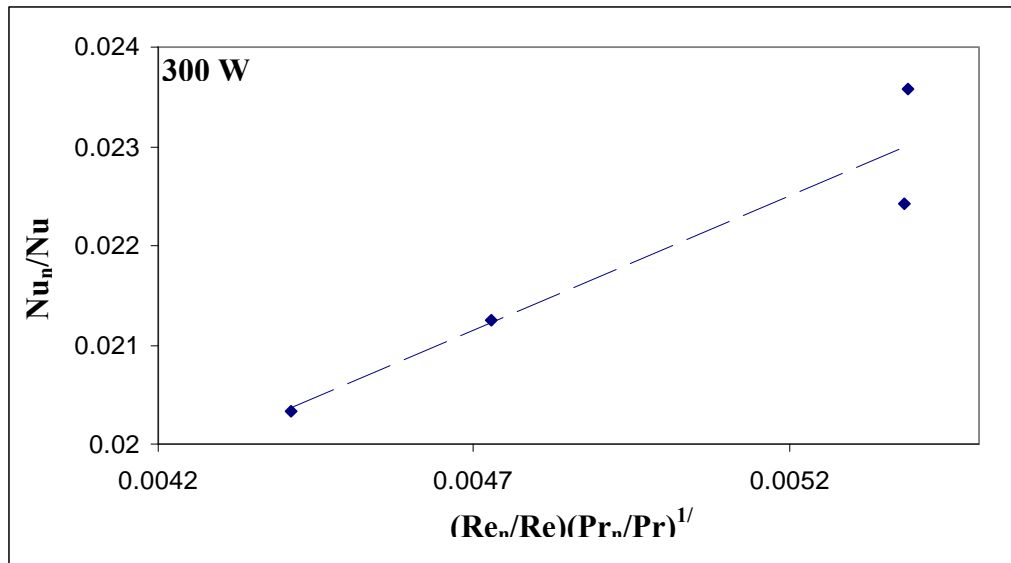


Figure 19. Comparison of the ratio of Nu and ratio of the  $(RePr^{1/3})$  at a 300 W input.

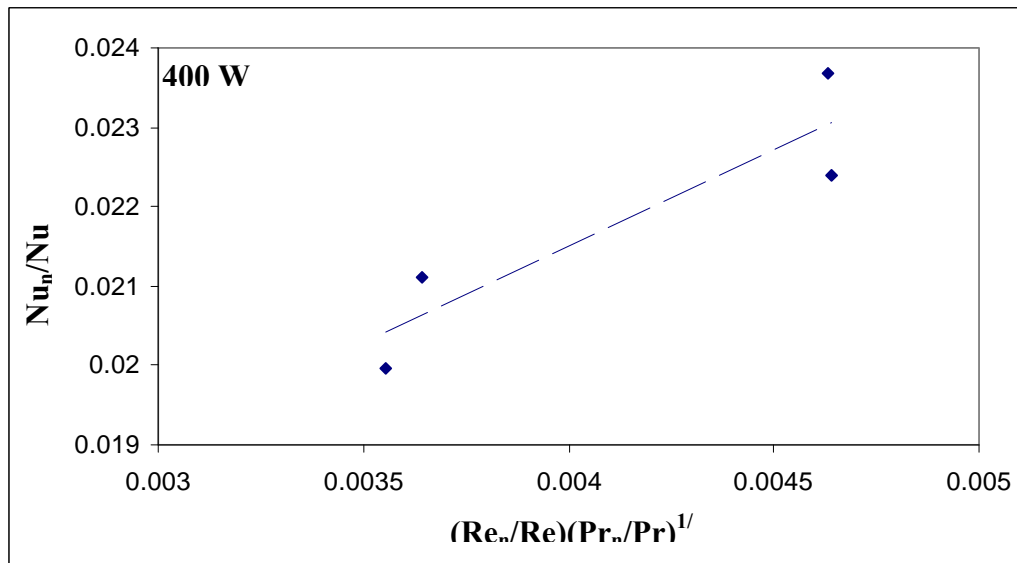
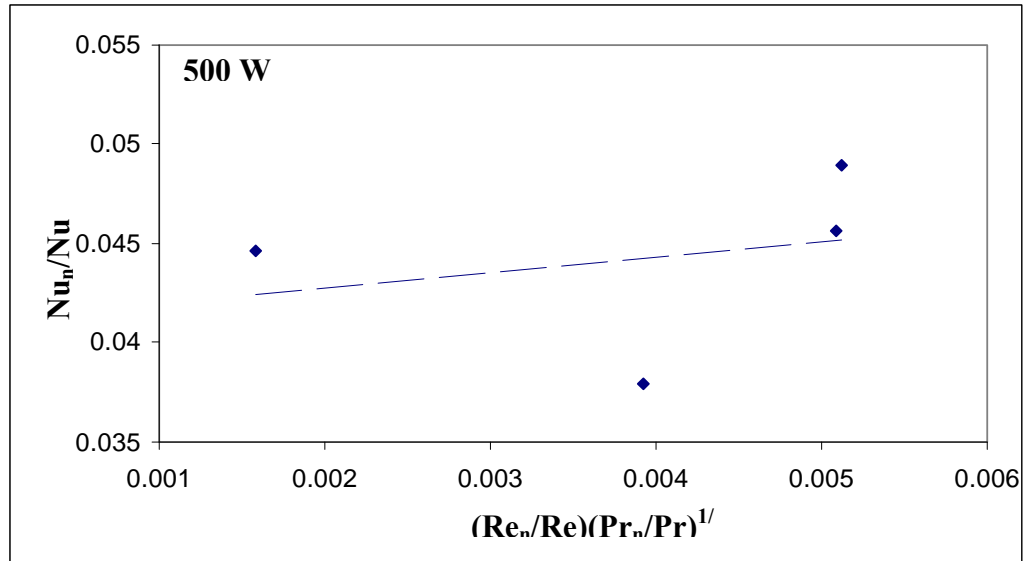


Figure 20. Comparison of the ratio of Nu and ratio of the  $(RePr^{1/3})$  at a 400 W input.



**Figure 21.** Comparison of the ratio of Nu and ratio of the  $(RePr^{1/3})$  at a 500 W input.

**Table 2.** Relationship between the ratio of Nu and ratio of the  $(RePr^{1/3})$  at 300 W input.

$Re_n/Re^*(Pr_n/Pr)^{1/3}$	$Nu_n/Nu$	Enhancement Ratio
0.0044	0.020	4.61
0.0047	0.021	4.50
0.0054	0.022	4.16
0.0054	0.024	4.38

**Table 3.** Relationship between the ratio of Nu and ratio of the  $(RePr^{1/3})$  at 400 W input.

$Re_n/Re^*(Pr_n/Pr)^{1/3}$	$Nu_n/Nu$	Enhancement Ratio
0.004	0.020	5.62
0.004	0.021	5.80
0.005	0.024	5.11
0.005	0.022	4.82

**Table 4.** Relationship between the ratio of Nu and ratio of the  $(RePr^{1/3})$  at 500 W input.

$Re_n/Re^*(Pr_n/Pr)^{1/3}$	$Nu_n/Nu$	Enhancement Ratio
0.004	0.038	9.67
0.002	0.045	28.20
0.005	0.046	8.98
0.005	0.049	9.57



## CHAPTER VI

### CONCLUSION

Experiments were performed using a flow loop experimental apparatus for poly-alpha-olefin (PAO) and nanofluid as coolants. The nanofluids were obtained by ultrasonically dispersing exfoliated graphite nanoparticles in PAO at two different nanofluid concentrations (0.3% and 0.6% by weight). Experiments were performed by varying the input power and the flow rates.

The thermophysical properties of the nanofluid (e.g., viscosity, thermal diffusivity, thermal conductivity and specific heat) were measured and were found to increase when compared to PAO. The heat flux in the cooling chamber of the flow loop was found to increase with increasing nanoparticle concentration and increasing flow rates for input power of 300W and 400W. SEM and EDX analysis of the heater surface in the cooling chamber show that nanoparticles were deposited on the heater surface. These results suggest that the precipitation of nanoparticles results in formation of enhanced heat transfer surfaces (nanofins), thereby enhancing the heat transfer to the bulk fluid. Such a transport mechanism is non-existent for experiments performed using PAO.

Anomalous heat fluxes were observed at input power of 500W. This is possibly due to higher surface temperature of the heater at this input power which caused localized coagulation of the nanofluids and agglomeration of the nanoparticles resulting in lower heat flux at lower flow velocities. Viscosity measurement data for the

nanofluids suggests that such coagulation of the nanofluids occurs at temperatures exceeding a threshold value of  $\sim 100$  °C.

## REFERENCES

1. Oberline, A., Endo, M., Koyama, T., "High Resolution Electron Microscope Observations of Graphitized Carbon Fibers," *Carbon*, Vol. 14, 1976, pp. 133-135.
2. Iijima, S., "Helical Microtubules of Graphite Carbon," *Letters to Nature*, Vol. 354, 1991, pp. 56-58.
3. Choi, S. U. S., Zhang, Z. G., Yu, W., Lockwood, F. E., Grulke, E. A., "Anomalous Thermal Conductivity Enhancement in Nanotube Suspensions," *Applied Physics Letters*, Vol. 79, No. 14, 2001, pp. 2252-2254.
4. You, S. M., Kim, J.H., Kim, K. H., "Effect of Nanoparticles on Critical Heat Flux of Water in Pool Boiling Heat Transfer," *Applied Physics Letters*, Vol. 83, No. 16, 2003, pp. 3374-3376.
5. Klebniski, P., Eastman, J.A., Cahill, D.G., "Nanofluids for Thermal Transport," *Materials Today*, Vol. 8, No. 6, 2005, pp. 36-44.
6. Lee, S., Choi, S.U. S., Li, S., Eastman, J.A., "Measuring Thermal Conductivity of Fluids Containing Oxide Nanoparticles," *Journal of Heat Transfer*, Vol. 121, No. 2, 1999, pp. 280-289.
7. Wang, X-Q., Mujumdar, A.S., "Heat Transfer Characteristics of Nanofluids: A Review," *International Journal of Thermal Sciences*, Vol. 46, 2007, pp. 1-19.
8. Eastman, J.A., Choi, S.U.S., Li, S., Yu, W., Thompson, L.J., "Anomalous Increase in Effective Thermal Conductivities of Ethylene Glycol-based Nanofluids Containing Copper Nanoparticles," *Applied Physics Letters*, Vol. 78, No. 6, 2001, pp. 718-720.
9. Hamilton, R.L., Crosser, O. K., "Thermal Conductivity of Heterogeneous Two-component Systems," *Industrial and Engineering Chemistry Fundamentals*, Vol. 1, 1962, pp. 187-191.
10. Choi, S. U. S., *Enhancing Thermal Conductivity of Fluids with Nanoparticles*, ASME, New York, 1995, pp. 99.
11. Lee, U. S. Choi, S. Li, and J. A. Eastman, *ASME J. Heat Transfer* 121, 280, 1999.
12. Xie, H., Wang, J., Xi, T., and Liu, Y., "Thermal Conductivity of Suspensions Containing Nanosized SiC Particles," *International Journal of Thermophysics*, Vol. 23, No. 2, 2002, pp. 571-580.

13. Prasher, R., Bhattacharyya, P., Phelan, P.E., "Brownian-Motion Based Convective-Conduction Model for Effective Thermal Conductivity of Nanofluids," *ASME Journal of Heat Transfer*, Vol. 128, 2006, pp. 588-595.
14. Putnam, S.A., Cahill, D.G., Braun, P.V., Ge, Z., Shimmin, G., "Thermal Conductivity of Nanofluid Suspension," *Journal of Applied Physics*, Vol. 99, Paper No. 084308, 2006.
15. Mills, A.F., *Heat and Mass Transfer*, 1995, Irwin Publishers, Boston.
16. Zhou, D. W., "Heat Transfer Enhancement of Copper Nanofluid with Acoustic Cavitation," *International Journal of Heat and Mass Transfer*, Vol. 47, 2004, pp. 3109-3117.
17. Das, S. K., Putra, N., Thiesen, P., Roetzel, W., "Temperature Dependence of Thermal Conductivity Enhancement for Nanofluids," *Journal of Heat Transfer*, Vol. 125, 2003, pp. 567-574.
18. Vassallo, P., Kumar, R., D'Amico, S., "Pool Boiling Heat Transfer Experiments in Silica-Water Nano-fluids," *International Journal of Heat and Mass Transfer*, Vol. 47, 2004, pp. 407-411.
19. Pak, B.C., Cho, Y.I., "Hydrodynamic and Heat Transfer Study of Dispersed Fluids with Sub-micron Metallic Oxide Particles," *Journal of Experimental Heat Transfer*, Vol. 11, No. 2, 1998, pp. 151-170.
20. Lee, S., Choi, S.U.S., Li, S., Eastman, J.A., "Measuring Thermal Conductivity of Fluids Containing Oxide Nanoparticles," *Journal of Heat Transfer*, Vol. 121, 1999, pp. 280.
21. Xuan, Y., Qiang, L., "Investigation on Convective Heat Transfer and Flow Features of Nanofluids," *Journal of Heat Transfer*, Vol. 125, 2003, pp. 151-155.
22. Wen, D., Ding, Y., "Experimental Investigation into Convection Heat Transfer of Nanofluids at the Entrance Region Under Laminar Flow Conditions," *International Journal of Heat and Mass Transfer*, Vol. 47, 2004, pp. 5181-5188.
23. Heris, S.Z., Etemad, S.Gh., Esfahany, M.N., "Experimental Investigation of Oxide Nanofluids at the Entrance Region Under Laminar Flow Conditions," *International Communications in Heat and Mass Transfer*, Vol. 33, 2006, pp. 529-535.

24. Lai, W.Y., Duculescu, B., Phelan, P., Prasher, R.S., "Convective Heat Transfer with Nanofluids in a Single 1.02 mm Tube," Proceedings of the 2006 ASME International Mechanical Engineering Congress and Exposition, Chicago, Illinois, 2006, Paper No. IMECE2006-14132.
25. Yang, Y., Zhang, Z.G., Grulke, E.A., Anderson, W.B., Wu, G., "Heat Transfer Properties of Nanoparticles-in-Fluid Dispersions (Nanofluid) in Laminar Flow," *International Journal of Heat and Mass Transfer*, Vol. 48, 2005, pp. 1107-1116.
26. Ding, Y., Alias, H., Wen, D., Williams, R. A., "Heat Transfer of Aqueous Suspensions of Carbon Nanotubes (CNT Nanofluids)," *International Journal of Heat and Mass Transfer*, Vol. 49, 2006, pp. 240-250.
27. Masuda, H., Ebata, A., Teramae, K., Hishinuma, N., "Alteration of Thermal Conductivity and Viscosity of Liquid by Dispersing Ultra-fine Particles," *Jpn. J. Thermophysics Properties*, Vol. 4, 1993, pp.227-233.
28. Eastman, J.A., Choi, U.S., Li, S. Thompson, L.J., Lee, S., "Enhanced Thermal Conductivity Through the Development of Nanofluids," Materials Research Society Symposium – Proceedings, Vol. 457, Materials Research Society, Pittsburgh, PA, USA, Boston, MA, USA, 1997, pp. 3-11.
29. Pak, B. C., and Cho, Y. I., "Hydrodynamic and Heat Transfer Study of Dispersed Fluids with Submicron Metallic Oxide Particles," *Experimental Heat Transfer*, Vol. 11, 1998, pp. 151-170.
30. Wang, X., Xu, X., Choi, S.U.S., "Thermal Conductivity of Nanoparticle-fluid Mixture," *Journal of Thermophysics and Heat Transfer*, Vol. 14, No. 4, 1999, pp. 474-480.
31. Eastman, J. A., Choi, S.U.S, Li, S., Soyez, G., Thompson, L.J., Di Melfi, R.J., "Novel Thermal Properties of Nanostructured Materials," *Material Science Forum*, 312-314, 1999, pp. 629-634.
32. Xie, H., Wang, J., Xi, T., Liu, Y., "Thermal Conductivity of Suspensions Containing Nanosized SiC Particles," *International Journal of Thermophysics*, Vol. 23, No. 2, 2002, pp. 571-580.
33. Xie, H., Wang, J., Xi, T., Liu, Y., "Study on the Thermal Conductivity of SiC Nanofluids," *Journal of the Chinese Ceramic Society*, Vol. 29, No. 4, 2001, pp. 361-364.

34. Xie, H., Wang, J., Xi, T., Liu, Y., Al, F., "Dependence of the Thermal Conductivity of Nanoparticle-fluid Mixture on the Base Fluid," *Journal of Materials Science Letters*, Vol. 21, 2002, pp. 1469-1471.
35. Zhou, L. P., and Wang, B. X., Annual Proceedings of Chinese Engineering in Thermophysics (in Chinese), Beijing, China, 2002, pp. 889.
36. Biercuk, M. J., Llaguno, M. C., Radosavljevic, M., Hyun, J. K., Johnson, A. T., "Carbon Nanotube Composites for Thermal Management," *Applied Physics Letters*, Vol. 80, No. 15, 2002, pp. 2767-2769.
37. Das, S.K., Putta, P., Thiesen, P., Roetzel, W., "Temperature Dependence of Thermal Conductivity Enhancement for Nanofluids," *ASME Trans. Journal of Heat Transfer*, Vol. 125, 2003, pp. 567-574.
38. Patel, H. E., Das, S. K., Sundararajan, T., "Thermal Conductivities of Naked and Monolayer Protected Metal Nanoparticle Based Nanofluids: Manifestation of Anomalous Enhancement and Chemical Effect," *Applied Physics Letters*, Vol. 83, No. 14, 2003, pp. 2931-2933.
39. Xie, H., Lee, H., Youn, W., Choi, M., "Nanofluids Containing Multiwalled Carbon Nanotubes and their Enhanced Thermal Conductivities," *Journal of Applied Physics*, Vol. 94, No. 8, 2003, pp. 4967-4971.
40. Choi, E.S., Brooks, J.S., Mehring, M., Roth, S., AIP Conference Proceedings, Vol. 591, Woodbury, NY, 2001.
41. Wen, D. S., Ding, Y. L., "Effective Thermal Conductivity of Aqueous Suspensions of Carbon Nanotubes," *Journal of Thermophysics and Heat Transfer*, Vol. 18, 2004, pp. 481-485.
42. Hong, T.-K., Yang, H.-S., Choi, C.J., "Study of the Enhanced Thermal Conductivity of Fe Nanofluids," *Journal of Applied Physics*, Vol. 97, No. 6, 2005, pp. 1-4.
43. Assael, M. J., Chen, C.R., Metaxa, I.N., Wakeam, W.A., Proceedings fo the 27<sup>th</sup> International Thermal Conductivity Conference and 15<sup>th</sup> International Thermal Expansion Symposium, edited by H. Wang and W.D. Porter (DES Tech Publications, Lancaster, PA), 2005, Vol. 153.
44. Wen, D., Ding, Y., "Formulation of Nanofluids for Natural Convective Heat Transfer Applications," *International Journal of Heat and Fluid Flow*, Vol. 26, No. 6, 2005, pp. 855-864.

45. Liu, M.S., Ching-Cheng Lin, M., Huang, I.T., Want, C.-C., "Enhancement of Thermal Conductivity with Carbon Nanotube for Nanofluids," *International Communications in Heat and Mass Transfer*, Vol. 32, No. 9, 2005, pp. 1202-1210.
46. Murshed, S.M.S, Leong, K.C., Yang, C., "Enhanced Thermal Conductivity of TiO<sub>2</sub>-water Based Nanofluids," *International Journal of Thermal Sciences*, Vol. 44, No.4, 2005, pp. 367-373.
47. Ghajar, A., Tang, W. and Beam, J., "Comparison of Hydraulic and Thermal Performance of PAO and Coolanol 25R Liquid Coolants," 6th AIAA/ASME Joint Thermophysics and Heat Transfer Conference, Colorado Springs, CO, June 20-23, 1994, pp. 1-14.
48. Lin, L., Ponnappan, R., Leland, J.E., "Heat Transfer Correlations For Plain Fin Array Cooler," AIAA Aerospace Sciences Meeting & Exhibit, 40<sup>th</sup>, Reno NV; 14-17 Jan. 2002.
49. Weiting, A. R., "Empirical Correlations for Heat Transfer and Flow Friction Characteristics of Rectangular Offset-Fin Plate-Fin Heat Exchangers," *ASME Journal of Heat Transfer*, Vol. 97, 1975, pp. 488-490.

**GLOSSARY**

CHF	Critical Heat Flux
MWNT	Multi-Walled Nanotubes
THW	Transient Hot Wire
Nu	Nusselt Number
Re	Reynolds Number
Pr	Prandtl Number
DW	Distilled Water
CNT	Carbon Nanotube
SEM	Scanning Electron Microscope
TEM	Transmission Electron Microscope
AFRL	Air Force Research Labs
PAO	Poly-Alpha-Olefin
EDX	Energy Dispersive X-Ray
DSC	Differential Scanning Calorimeter



**APPENDIX**


**MSDS FOR PAO**



## Material Safety Data Sheet


<b>Section 1. Chemical product and company identification</b>			
<b>Common name</b>	<b>BRAYCO MICRONIC 889</b>	<b>Code</b>	0000001487 (27019-AW)
<b>Supplier</b>	Air BP Lubricants Maple Plaza II - 1N Six Campus Drive Parsippany, NJ 07054 U.S.A.(973)401-4350	<b>Validation date</b>	03/12/2004
		<b>Print date</b>	03/12/2004
<b>Synonym</b>	Not available.	<b>Responsible name</b>	Product Stewardship
<b>Trade name</b>	BRAYCO IS A TRADEMARK OF CASTROL	<b>In case of emergency</b>	CHEMTREC (800) 424-9300
<b>Material uses</b>	Industrial applications		
<b>Manufacturer</b>	CASTROL INDUSTRIAL NORTH AMERICA INC 1001 WEST 31ST STREET DOWNERS GROVE, IL 60515-1280		
<b>Section 2. Composition, Information on Ingredients</b>			
Name	CAS #	% by weight	Exposure limits
1-DECENE, DIMER, HYDROGENATED	68649-11-6	60-100	Not available.
<b>Section 3. Hazards identification</b>			
<b>Physical state / Appearance</b>	Liquid.		
<b>Odor (Slight.)</b>	Red liquid. (Dark.)		
<b>Emergency overview</b>	<p><b>WARNING!</b></p> <p>HARMFUL IF INHALED. ASPIRATION HAZARD. MAY CAUSE ADVERSE LUNG EFFECTS IF HIGH CONCENTRATIONS ARE INHALED. MAY CAUSE RESPIRATORY TRACT IRRITATION.</p> <p>Do not breathe vapor or mist. Aspiration hazard if swallowed -- harmful or fatal if liquid is aspirated into lungs. Do not ingest. If ingested do not induce vomiting. Wash thoroughly after handling. Avoid contact with skin and eyes. However, in light of good industrial hygiene, exposure to any chemical should be kept to a minimum. Keep away from heat, sparks and flame.</p>		
<b>Routes of Entry</b>	Skin Contact. Eye contact. Inhalation. Ingestion.		
<b>Potential acute health effects</b>	<p><b>Eyes</b> No significant health hazards identified.</p> <p><b>Skin</b> No significant health hazards identified.</p> <p><b>Inhalation</b> Vapor: Prolonged repeated exposure may cause chemical pneumonitis. Exposure to aerosols or particulates from heated material may cause adverse lung effects if high concentrations are inhaled.</p> <p><b>Ingestion</b> Aspiration hazard if swallowed- can enter lungs and cause damage.</p> <p>No additional remark.</p>		
<b>Continued on next page</b>			

<b>BRAYCO MICRONIC 889</b>		<i>Page: 2/7</i>
<b>Potential chronic health effects</b>	<p><b>CARCINOGENIC EFFECTS:</b> No component of this product at levels greater than 0.1% is identified as a carcinogen by ACGIH or the International Agency for Research on Cancer (IARC). No component of this product present at levels greater than 0.1% is identified as a carcinogen by the U.S. National Toxicology Program (NTP) or the U.S. Occupational Safety and Health Act (OSHA).</p> <p><b>MUTAGENIC EFFECTS:</b> No component of this product at levels greater than 0.1% is classified by established regulatory criteria as a mutagen.</p> <p><b>TERATOGENIC EFFECTS:</b> No component of this product at levels greater than 0.1% is classified by established regulatory criteria as teratogenic or embryotoxic.</p>	
<b>Medical conditions aggravated by overexposure:</b>	Repeated or prolonged exposure is not known to aggravate medical condition.	
<b>Over-exposure signs/symptoms</b>	Not available.	
See toxicological Information (section 11)		
<b>Section 4. First aid measures</b>		
<b>Eye Contact</b>	Flush with plenty of water for at least 15 minutes, occasionally lifting the upper and lower eyelids. Get medical attention.	
<b>Skin Contact</b>	Wash contaminated skin with soap and water. Get medical attention if irritation develops. Wash clothing before reuse.	
<b>Inhalation</b>	Breathing difficulty or Respiratory tract irritation: Remove to fresh air. If the victim is not breathing, perform mouth-to-mouth resuscitation. If breathing is difficult, give oxygen. Get medical attention immediately.	
<b>Ingestion</b>	ASPIRATION HAZARD. Do not induce vomiting. If vomiting occurs, keep head lower than hips to help prevent aspiration. If affected person is conscious, give plenty of water to drink. NEVER give an unconscious person anything to ingest. Get medical attention immediately.	
<b>Notes to Physician</b>	Not available.	
<b>Section 5. Fire fighting measures</b>		
<b>Flammability of the product</b>	May be combustible at high temperature.	
<b>Auto-ignition temperature</b>	Not available.	
<b>Flash Point</b>	Open cup: 166°C (330.8°F) (Cleveland.).	
<b>Flammable limits</b>	Not available.	
<b>Products of combustion</b>	These products are carbon oxides (CO, CO <sub>2</sub> ).	
<b>Fire hazards in presence of various substances</b>	Slightly flammable to flammable in presence of open flames, sparks and static discharge, of shocks, of heat, of oxidizing materials.	
<b>Explosion hazards in presence of various substances</b>	This material is not explosive as defined by established regulatory criteria.	
<b>Fire Fighting Media and Instructions</b>	<p>SMALL FIRE: Use DRY chemical powder.</p> <p>LARGE FIRE: Use water spray, fog or foam.</p> <p>Cool closed containers exposed to fire with water. Hot containers may explode. Use water spray to keep fire exposed containers cool. Do not use water jet.</p>	
<b>Protective clothing (fire)</b>	Fire fighters should wear positive pressure self-contained breathing apparatus (SCBA) and full turnout gear.	
<b>Special remarks on fire hazards</b>	None identified.	
<b>Continued on next page</b>		

<b>BRAYCO MICRONIC 889</b>		<i>Page: 3/7</i>
<b>Special remarks on explosion hazards</b>	None identified.	
<b>Section 6. Accidental release measures</b>		
<b>Small spill and leak</b>	Absorb with an inert material and put the spilled material in an appropriate waste disposal. Do not allow any potentially contaminated water including rain water, runoff from fire fighting or spills to enter any waterway, sewer or drain.	
<b>Large spill and leak</b>	Absorb with an inert material and put the spilled material in an appropriate waste disposal. Do not allow any potentially contaminated water including rain water, runoff from fire fighting or spills to enter any waterway, sewer or drain.	
<b>Section 7. Handling and storage</b>		
<p>Aerosol.: Over-exposure by inhalation may cause respiratory irritation. However, in light of good industrial hygiene, exposure to any chemical should be kept to a minimum. Do not ingest. Avoid contact with eyes, skin and clothing. Wash thoroughly after handling.</p> <p>Keep container tightly closed. Keep container in a cool, well-ventilated area. Empty containers may contain harmful, flammable/combustible or explosive residue or vapors. Do not cut, grind, drill, weld, reuse or dispose of containers unless adequate precautions are taken against these hazards.</p>		
<b>Section 8. Exposure Controls and Personal Protection</b>		
<b>Engineering controls</b>	Aerosol.: Over-exposure by inhalation may cause respiratory irritation. Provide exhaust ventilation or other engineering controls to keep the airborne concentrations of vapors below their respective occupational exposure limits. However, in light of good industrial hygiene, exposure to any chemical should be kept to a minimum.	
<b>Personal protection</b>	<p><b>Eyes</b> Safety glasses with side shields. OR Chemical splash goggles.</p> <p><b>Body</b> Avoid prolonged or repeated contact with skin. Wear clothing and footwear that cannot be penetrated by chemicals or oil.</p> <p><b>Respiratory</b> A respirator is not needed under normal and intended conditions of product use. Wear appropriate respirator when ventilation is inadequate. If heated and ventilation is inadequate, use a NIOSH certified respirator with an organic vapor cartridge and P95 particulate filter.</p> <p><b>Hands</b> Impervious gloves.</p> <p><b>Feet</b> Not applicable.</p>	
<b>Protective clothing (pictograms)</b>		
<b>Personal protection in case of a large spill</b>	Splash goggles. Full suit. Boots. Gloves. Suggested protective clothing might not be sufficient; consult a specialist BEFORE handling this product.	
<b>Product Name</b>	<b>Exposure limits</b>	
1-DECENE, DIMER, HYDROGENATED	Not available.	
<b>Consult local authorities for acceptable exposure limits.</b>		
<b>Continued on next page</b>		

<b>BRAYCO MICRONIC 889</b>		<b>Page: 4/7</b>	
<b>Section 9. Physical and chemical properties</b>			
Physical state / Appearance	Liquid.	Odor	Odor (Slight.)
Boiling/condensation point	Not available.	Taste	Not available.
Melting/freezing point	Not available.	Color	Red liquid. (Dark.)
pH ( Concentration )	Not applicable.		
pH Dilution % and Value	Not Applicable		
Critical temperature	Not available.		
Specific Gravity	0.82 to 0.84 (Water = 1)		
Vapor pressure	Not available.		
Vapor density	Not available.		
Volatility	Not available.		
Odor threshold	Not available.		
Evaporation rate	Not available.		
VOC	Not available.	VOC Method	Not available.
Viscosity	Kinematic (40C): 5.1 cSt		
Dispersion properties	Is not dispersed in cold water, hot water.		
Solubility	Insoluble in cold water, hot water.		
Physical chemical comments	Not available.		
<b>Section 10. Stability and reactivity</b>			
Stability and Reactivity	The product is stable.		
Conditions of instability	Avoid excessive heat.		
Incompatibility with various substances	Strong oxidizing materials		
Hazardous Decomposition Products	carbon oxides (CO, CO2), sulfur oxides (SO2, SO3...), nitrogen oxides (NO, NO2...)		
Hazardous polymerization	Will not occur.		
<b>Section 11. Toxicological information</b>			
Toxicity to animals	Acute toxicity of the vapor (LC50): 1.17 mg/l 4 hour(s) [Rat]. (Poly-alpha-olefin). Special remarks on toxicity to animals.		
Chronic effects on humans			
<b>Continued on next page</b>			



<b>BRAYCO MICRONIC 889</b>		<b>Page: 5/7</b>
	<p>Prolonged or repeated contact can defat the skin and lead to irritation and/or dermatitis.  <b>CARCINOGENIC EFFECTS:</b> No component of this product at levels greater than 0.1% is identified as a carcinogen by ACGIH or the International Agency for Research on Cancer (IARC). No component of this product present at levels greater than 0.1% is identified as a carcinogen by the U.S. National Toxicology Program (NTP) or the U.S. Occupational Safety and Health Act (OSHA).  <b>MUTAGENIC EFFECTS:</b> No component of this product at levels greater than 0.1% is classified by established regulatory criteria as a mutagen.  <b>TERATOGENIC EFFECTS:</b> No component of this product at levels greater than 0.1% is classified by established regulatory criteria as teratogenic or embryotoxic.  <b>REPRODUCTIVE EFFECTS:</b> No component of this product at levels greater than 0.1% is classified by established regulatory criteria as a reproductive toxin.</p>	
<b>Other Toxic Effects on Humans</b>	Aspiration hazard if swallowed- can enter lungs and cause damage.	
<b>Special remarks on toxicity to animals</b>	The air concentration at which this study was conducted was extremely high and is not typically encountered under normal conditions of use.	
<b>Special remarks on chronic effects on humans</b>	No additional remark.	
<b>Special Remarks on Other Toxic Effects on Humans</b>	No additional remark.	
<b>Section 12. Ecological information</b>		
<b>Ecotoxicity</b>	Not determined.	
<b>BOD and COD</b>	Not determined.	
<b>Biodegradable/OECD</b>	Not determined.	
<b>Mobility</b>	Not determined.	
<b>Products of degradation</b>	carbon oxides (CO, CO <sub>2</sub> ), sulfur oxides (SO <sub>2</sub> , SO <sub>3</sub> ...), nitrogen oxides (NO, NO <sub>2</sub> ...)	
<b>Toxicity of the products of biodegradation</b>	Not determined.	
<b>Special remarks on the products of biodegradation</b>	No additional remark.	
<b>Section 13. Disposal considerations</b>		
<b>Waste information</b>	Waste must be disposed of in accordance with federal, state and local environmental control regulations. Keep out of waterways. Disposal of this material to the land may be banned by federal law (40 CFR 268).	
<b>RCRA Waste Code(s)</b>	USED OIL	
<b>Waste stream</b>	Not determined.	
<b>Consult your local or regional authorities.</b>		
<b>Section 14. Transport information</b>		
<b>DOT Classification</b>	Not a DOT controlled material (United States).	
<b>Marine Pollutant</b>	Not pollutant.	
<b>Continued on next page</b>		

<b>BRAYCO MICRONIC 889</b>		<i>Page: 6/7</i>
<b>Special Provisions for Transport</b>	NOT REGULATED	
<b>ADR/RID Classification</b>	Not determined.	
<b>IMO/IMDG Classification</b>	Not determined.	
<b>ICAO/IATA Classification</b>	Not determined.	

### Section 15. Regulatory information

#### U.S. Federal regulations

SARA 302/304 emergency planning and notification: No products were found.  
 SARA 311/312 MSDS distribution - chemical inventory - hazard identification: BRAYCO MICRONIC 889: immediate health hazard.  
 SARA 313 toxic chemical notification and release reporting: No products were found.

Clean Water Act (CWA) 307: No products were found.  
 Clean Water Act (CWA) 311: No products were found.  
 Clean air act (CAA) 112 accidental release prevention: No products were found.  
 Clean air act (CAA) 112 regulated toxic substances: No products were found.  
 Clean air act (CAA) 112 regulated flammable substances: No products were found.

#### State regulations

No products were found.  
 California prop. 65: No products were found.

#### Inventory Lists

TSCA 8(b) inventory: In compliance.  
 CEPA DSL: In compliance.  
 Australia (NICNAS): In compliance.  
 Korea (TCCL): In compliance.  
 Philippines (RA6969): In compliance.  
 MITI: In compliance.  
 EINECS: In compliance.

### Section 16. Other information

#### Label Requirements

HARMFUL IF INHALED.  
 ASPIRATION HAZARD.  
 MAY CAUSE ADVERSE LUNG EFFECTS IF HIGH CONCENTRATIONS ARE INHALED.  
 MAY CAUSE RESPIRATORY TRACT IRRITATION.

#### Hazardous Material Information System (U.S.A.)

Health	1
Fire hazard	1
Reactivity	0
Personal protection	X

**National Fire Protection Association (U.S.A.)**



#### References

Not available.

**Continued on next page**

<b>BRAYCO MICRONIC 889</b>		<i>Page: 7/7</i>
<b>Other special considerations</b>	PETROLEUM OIL: STEL = 10 mg/M3. Using terminology of the International Agency for Research on Cancer (IARC), the petroleum distillates listed in Section II are classified by the supplier as severely processed. Not all those listed in Section II may be present. The supplier has stated that these distillates do not require a carcinogen label as defined by OSHA 29 CFR 1910.1200.	
Validated by Product Stewardship on 03/12/2004.		Printed . (PrintDate(03/12/2004.
CHEMTREC (800) 424-9300		
<b><u>Notice to reader</u></b> <i>To the best of our knowledge, the information contained herein is accurate. However, neither the above named supplier nor any of its subsidiaries assumes any liability whatsoever for the accuracy or completeness of the information contained herein. Final determination of suitability of any material is the sole responsibility of the user. All materials may present unknown hazards and should be used with caution. Although certain hazards are described herein, we cannot guarantee that these are the only hazards that exist.</i>		



## VITA

Name: Ian Carl Nelson

Address: Department of Mechanical Engineering,  
Texas A&M University,  
College Station,  
Texas – 77843-3123

Education: M.S., Mechanical Engineering, Texas A&M University,

Aug. 2007.

B.S., Mechanical Engineering, The University of Texas,

Dec. 2004.

Publications:

1. I.C. Nelson, D. Banerjee, “Detection of Explosives Using Micro-Cantilever Based Sensors.” *SPIE Proceedings of Defense and Security Symposium 2006*, Orlando, Florida, April 17, 2006.